University of Crete
Department of Materials Science and Technology

Master Thesis

Theoretical Investigation of Tungsten Disulfide – Graphene Heterostructures

Author
Kanakis Stavroulakis

Supervisor
Assoc. Prof. George Kopidakis

Heraklion Crete

October 2017

MSc THESIS

A thesis submitted in fulfillment of the requirements for the degree of Master of Science in Materials Science and Technology

Defended by Kanakis Stavroulakis

Theoretical Investigation of Tungsten Disulfide - Graphene Heterostructures

COMMITTEE

Assoc. Prof. George Kopidakis

Assoc. Prof. George Kioseoglou

Asst. Prof. Ioannis Remediakis

"If you can't explain it simply,
you don't understand it well enough."

Albert Einstein & Richard Feynman

«Theoretical investigation of tungsten disulfide - graphene heterostructures»

Abstract

Research in two-dimensional (2D) materials and van der Waals heterostructures gains enormous popularity across various scientific and engineering disciplines. Electrons in these materials can move in two dimensions but are confined in the out of plane direction, leading to some fascinating optoelectronic properties. In this direction of research, we present Density Functional Theory (DFT) results for the atomic and electronic structure of WS_2 monolayer, graphene and WS_2/graphene heterobilayer. We performed DFT calculations to investigate interlayer interactions and the effect of lattice mismatch in WS_2/graphene van der Waals heterostructures. We found that strain affects their binding energy and electronic structure. Examining stability and band alignment in these heterostructures with DFT is quite challenging. By using different WS_2/graphene supercells with different lattice mismatch and by unfolding their electronic band structure, we find that strain induces significant electronic properties modifications in the WS_2 layer, such as direct to indirect band gap transitions. Furthermore, in an effort to interpret recent experiments, we studied exciton effects in WS_2 monolayer using theoretical methods based on the Bethe-Salpeter equation (BSE) for 2D materials. Our excitonic spectra are in good agreement with experimental data and are affected by strain in a way which is consistent with confinement effects. Theoretical understanding of the optoelectronic properties of WS_2/graphene heterostructures complements experimental works and provides a powerful tool for exploring potential applications and devices.

«Θεωρητική μελέτη ετεροδομών διθειούχου βολφραμίου - γραφενίου»

Περίληψη

Η έρευνα στα δισδιάστατα (2Δ) υλικά και στις ετεροδομές van der Waals έχει γίνει εξαιρετικά δημοφιλής σε διάφορα πεδία της επιστήμης και της μηχανικής. Τα ηλεκτρόνια στα υλικά αυτά μπορούν να κινούνται σε δύο διαστάσεις αλλά είναι περιορισμένα στην εκτός επιπέδου διεύθυνση, με αποτέλεσμα να παρουσιάζουν ορισμένες εντυπωσιακές οπτοηλεκτρονικές ιδιότητες. Σε αυτή την ερευνητική κατεύθυνση, παρουσιάζουμε αποτελέσματα Θεωρίας Συναρτησιακού Πυκνότητας (Density Functional Theory - DFT) για την ατομική και ηλεκτρονική δομή της μονής στρώσης WS_2, του γραφενίου και της ετεροδομής διπλής στρώσης WS_2/γραφενίου. Πραγματοποιήσαμε υπολογισμούς DFT για να διερευνήσουμε τις δια-στρωματικές αλληλεπιδράσεις και την επίδραση της αναντιστοιχίας πλέγματος στις ετεροδομές van der Waals WS_2/γραφενίου. Διαπιστώσαμε ότι η παραμόρφωση επηρεάζει την ενέργεια δέσμευσης και την ηλεκτρονική δομή τους. Η μελέτη με DFT της σταθερότητας και της διάταξης των ηλεκτρονικών ζωνών σε τέτοιου είδους ετεροδομές παρουσιάζει αρκετές δυσκολίες. Χρησιμοποιώντας διαφορετικές υπερ-κυψελίδες WS_2/γραφενίου με διαφορετική αναντιστοιχία πλέγματος και ξεδιπλώνοντας την δομή των ηλεκτρονικών ζωνών τους, βρίσκουμε ότι η παραμόρφωση προκαλεί αξιοσημείωτες τροποποιήσεις των ηλεκτρονικών ιδιοτήτων στο στρώμα WS_2, όπως μεταβάσεις από άμεσο σε έμμεσο ενεργειακό χάσμα ζώνης. Επιπλέον, σε μια προσπάθεια να ερμηνεύσουμε πρόσφατα πειράματα, μελετήσαμε εξιτονικά φαινόμενα στο στρώμα WS_2 χρησιμοποιώντας θεωρητικές μεθόδους που βασίζονται στην εξίσωση Bethe-Salpeter (BSE) για 2Δ υλικά. Τα εξιτονικά φάσματα που υπολογίζουμε είναι σε συμφωνία με πειραματικά δεδομένα και επηρεάζονται από την παραμόρφωση με τρόπο που συνάδει με φαινόμενα κβαντικού περιορισμού. Η θεωρητική κατανόηση των οποτηλεκτρονικών ιδιοτήτων των ετεροδομών WS_2/γραφενίου συμπληρώνει τις πειραματικές εργασίες και παρέχει ένα ισχυρό εργαλείο για την διερεύνηση πιθανών εφαρμογών και συσκευών.

Acknowledgments

I would like to express my highest appreciation to my supervisor, Prof. George Kopidakis, for his support and careful guidance during my postgraduate studies. His vast knowledge of physics, as well as his ability to simplify the difficult concepts, help me to form deeper insights into physics. Furthermore, it is also important to thank Prof. Stamatis Stamatiadis for technical support at various times during the period of this work. I would like to thank all the members of materials theory group, especially Daphne Davelou, Mike Minotakis, Nick Vrithias for their comments and suggestions. I thank my close friends for their help. With Spyros Georgakis, Marios Savvakis, Manos Kokarakis, Aris Plexidas, Manos Archontakis we had a wonderful time and funny moments in the Heraklion all these years. Last but not least, I would like to express my sincere gratitude to my family and dedicate this thesis to them. It was impossible to achieve this task without the encouragement and the love of my parents.

Table of Contents

Chapter 1

Introduction

The study of two-dimensional (2D) layered materials has motivated enormous research activity, because electrons in these materials are absolutely confined in the out of plane direction leading to some very interesting quantum physics arising from their 2D nature. In this work, two of the most interesting 2D materials for optoelectronic applications are investigated, graphene and a semiconducting transition metal dichalcogenide (TMD), namely tungsten disulfide (WS_2). Separate layers of these 2D materials can be stacked vertically due to weak van der Waals (vdW) interactions, which allow the formation of heterostructures.

In this thesis, we provide theoretical calculations using Density Functional Theory (DFT) for understanding the atomic and electronic structure of these 2D materials and WS_2/graphene heterostructures, as well as excitonic effects in WS_2 monolayer. Such materials make highly suitable ingredients for components of next generation nanoelectronics devices, and give rise to new physical phenomena[1].

1.1 Two-Dimensional Materials

Two-dimensional (2D) materials, often referred to as "single layer materials", are crystalline materials consisting of a single layer of atomic thickness. One of the most famous of these 2D materials is graphene[2], which is a single layer of graphite in which the carbon atoms form a hexagonal honeycomb lattice. Since the isolation of graphene in 2004 a large amount of research has been directed in the study of these materials[19] and in 2010 the Nobel Prize was awarded to Andre Geim and Konstantin Novoselov[5]. Graphene shows outstanding properties such as very high carrier mobilities, excellent heat conductivity, and superior mechanical strength. Because of its remarkable properties[2][6][50], applications using graphene are developed in a wide range of areas, including high-speed electronics[7][9] and optical devices[8], energy generation and storage[10][11], hybrid materials[12], chemical sensors[13], and even DNA sequencing[14][15][16].

On the other hand, some of the most popular layered materials are the transition metal dichalcogenides (TMDs) such as MoS_2 and WS_2[17][18]. TMD monolayers are atomically thin semiconductors of the general type MX_2 where M is the transition metal atom and X is the chalcogen atom. This structure consists of a layer of transition metal among two layers of chalcogen. TMDs have attracted a lot of interest in the post graphene layered material era due to their significant optoelectronic properties[3][4][18]. TMD materials have the advantage over graphene of having extended bandgap tunability through composition, thickness and possibly even strain control. Semiconducting TMDs have a direct gap and can be used in electronics as transistors and in optics as emitters and detectors[20][21]. Two-dimensional nanomaterials composed of

graphene and nanostructured TMDs have attracted a great deal of interest due to their unique properties. Heterostructures of these materials are good candidates for potential applications in electronic devices such as solar cells, transistors and as a catalyst for hydrogen evolution in water splitting[22][60][68][69].

1.2 Computational science

Computational science describes the crucial role of computer as an effective tool in science and engineering. It includes many algorithms and models in order to solve huge and difficult problems which is impossible to manage by a human.

Materials science problems often require the solution of hard, frequently non-solvable via analytical methods equations. It is impossible to analytically solve most models that consider more than two bodies, except for a few special cases. This is very inconvenient because most interesting problems in condensed matter physics consider N particles, where N can be anything from a few hundreds to 10^{23}. Therefore, we need computational science which is the science that uses the numerical analysis in order to solve a problem for which a quantitative theory already exists.

In this case, the modelling method which we use is DFT, as we will discuss in the next chapter. The role of computational science in this thesis is the necessary tool for developing and implementing modelling at the atomistic level for understanding and predicting the atomic structure and the electronic properties of 2D materials.

1.3 Thesis Outline

In this thesis, we study the monolayer of WS_2, a material in the TMDs family, and well-known graphene, which is composed of a single sheet of carbon atoms arranged in a honeycomb lattice. We performed DFT calculations for the atomic structure and electronic band structure, first separately for the monolayer of WS_2 and graphene, and then for WS_2/Graphene heterostructure in order to analyze the optoelectronic properties.

The aim of this thesis is to investigate the WS_2/Graphene heterostructures and especially explore atomic structure and electronic band structure. To achieve this goal, we built two different sizes of supercell (SC). The heterostructure of WS_2 (3×3)/Graphene (4×4) with 59 atoms and the heterostructure of WS_2 (4×4)/Graphene (5×5) with 98 atoms in order to achieve a small lattice mismatch (approximately 1%) which plays a crucial role in the stability of the heterostructure. The strain in WS_2/Graphene heterostructures affects dramatically the electronic band structure picture. It is challenging to explain the behavior of band alignment in the electronic band structure diagrams. Furthermore, we performed calculations to examine the interlayer distance and the optimal configurations.

Finally, we studied the photoluminesce spectrum using the Bethe-Salpeter equation (BSE) in 2D systems and calculated excitonic effects in monolayer WS_2. The reason we study these heterostructures is to gain further knowledge from a theoretical point of view about the electronic properties and to complement or confirm experimental

works in these systems. These heterostructures have not been extensively studied and have prospects that may enable their widespread use in applications.

According to the above, this thesis is organized as follows: after this small introductory chapter 1, we give, in chapter 2, a brief overview of DFT and theoretical background behind the electronic band structure calculations. We also discuss, the basic concepts of the theory of BSE and last, we give some computational details. Later on, in chapter 3, we examine monolayer WS_2 and graphene and we present the results for their atomic and electronic structure from DFT calculations.

In chapter 4 we present the extensive study for WS_2/Graphene heterostructure and we give the results from DFT calculations for the atomic and electronic structure for different sizes of supercell (SC). We will analyze and discuss each case and explain the role of lattice mismatch on WS_2/Graphene heterostructures. In chapter 5, we will investigate the optical excitations in monolayer of WS_2 according to the spectrum from the BSE. In chapter 6, we give the conclusions of this thesis and we discuss the recent experimental works and future prospects in these vdW heterostructures.

Chapter 2

Theoretical and computational methods

In this thesis we use the Density Functional Theory (DFT). In this chapter, we will briefly discuss DFT and some of its important concepts. We describe the method which we follow for the electronic band structure calculations in the primitive cell (PC) and give an overview of the theory for electronic band structure unfolding for supercell (SC) calculations. We discuss the basic theory of the Random Phase Approximation (RPA) and Bethe-Salpeter Equation (BSE), which are the main methods we use for excitonic effects. Finally, in the last subsection, we give some computational details.

2.1 Density Functional Theory (DFT)

The introduction of quantum mechanics led to a revolution in science and is regarded as the most profound scientific breakthrough of all time. Quantum mechanics explains the behavior of matter and interactions on atomic scales. Every quantum mechanical phenomenon is described by the Schrödinger equation. DFT is a method in quantum mechanical modeling for studying the behavior of the material by solving the Schrödinger equation and finding the ground state of the system which is defined as the state in which the system has the lowest possible energy. On the other hand, excited state of a quantum mechanical system is any state that has energy greater than the ground state.

DFT is now one of the most dominant computational methods for electronic structure calculations as well as a tool for many-body problems in solid state physics and materials science. DFT was introduced by Hohenberg and Kohn in 1964[23] and the approximation of the many electron problem arose with results from the work of Hohenberg, Kohn and Sham[24]. The Hohenberg-Kohn theorem asserts that the electronic density of a system determines all ground state properties of the system. In this case, the total ground state energy of a many-electron system is a functional of the density. So, if we know the electron density functional, we know the total energy of our system. Based on these, the basic idea of DFT is to describe an interacting system of fermions via its density and not via its many-body wave function.

In DFT, the electronic orbitals are solutions to a Schrödinger equation which depends on the electron density rather than on individual electron orbitals. An assumption it uses in order to reduce as far as possible the number of degrees of freedom of the system is called the Born-Oppenheimer approximation. The Born-Oppenheimer approximation, in a few words, says that nuclei are fixed and the kinetic energy is a function of the electrons kinetic energy. This assumption is made because the nucleus is much heavier than the electron so it is clear that nuclei move much slower than electrons.

DFT applies to many-body systems and considers the interaction between electrons and nuclei. Nowadays, most atomic and electronic band structure calculations are based on DFT. At this point, some very basic concepts of quantum mechanics that the DFT uses are summarized.

Schrödinger equation, is a partial differential equation that describes the behavior of the quantum state of a physical system. This equation may be independent or dependent on time, and it has the general form:

$$\hat{H}\Psi = E\Psi \quad (1)$$

where $\hat{H}$ is the hamiltonian operator and Ψ is the wavefunction.

We can write the hamiltonian operator:

$$\hat{H} = \hat{T}_e + \hat{V}_{n-e} + \hat{V}_{e-e} \quad (2)$$

where $\hat{T}_e$ is the operator for the kinetic energy of electron, $\hat{V}_{n-e}$ is the operator for the potential energy through the Coulomb interactions of the nucleus and electron, $\hat{V}_{e-e}$ is the operator for the potential energy through Coulomb interaction of the electrons.

If we replace the expressions for the terms of equation we have:

$$\hat{H} = -\frac{\hbar^2}{2m_e}\sum_i \nabla_i^2 - \frac{e}{8\pi\varepsilon_0}\sum_{ij}\frac{Q_i}{|\vec{r_i}-\vec{R_j}|} + \frac{e^2}{8\pi\varepsilon_0}\sum_{ij}\frac{1}{|\vec{r_i}-\vec{r_j}|} \quad (3)$$

The fundamental axiom of DFT is that any property of a system of many interacting particles can be viewed as a functional of the electron density $n(\vec{r})$, which for a normalized Ψ is given by

$$n(\vec{r}) = N\int d^3r_2 \dots \int d^3r_N \Psi^*(\vec{r},\vec{r}_2,\dots,\vec{r}_N)\Psi(\vec{r},\vec{r}_2,\dots,\vec{r}_N) \quad (4)$$

where N is the total number of electrons and the total energy of the system can be determined by the expectation value of the hamiltonian:

$$E[n] = \langle\Psi[n]\big|\hat{T}_e + \hat{V}_{n-e} + \hat{V}_{e-e}\big|\Psi[n]\rangle \quad (5)$$

Minimizing the energy functional $E[n]$ with respect to $n(\vec{r})$ yields the ground state density.

The Kohn–Sham equations (non-interacting system):

$$\left[-\frac{\hbar^2}{2m_e}\sum_i \nabla_i^2 - \frac{e^2}{8\pi\varepsilon_0}\sum_i\frac{Z_i}{|\vec{r}-\vec{R}_i|} + \int d^3r' n(\vec{r'})\frac{1}{|\vec{r}-\vec{r'}|} + V_{xc}[n](\vec{r})\right]\psi_\iota(\vec{r}) = E_i\psi_\iota(\vec{r}) \quad (6)$$

yields orbitals ψ_ι that produce the density of the original system.

The fourth term of the hamiltonian, the exchange correlation potential, contains the many body effects. This term is the most important in DFT because it corrects for the

electron self-interaction which leads to the overestimated electron-electron interaction. There are no simple accurate expressions for exchange correlation potential. In order to calculate it some approximations are made and for that reason many functionals have been developed, such as the Generalized Gradient Approximation (GGA), Local Density Approximation (LDA).
For the purpose of this thesis we will use the LDA functional. LDA was formulated based on the properties of the uniform electron gas, and, therefore, it is exact for the special case of a uniform electronic system. LDA is a class of approximations for the exchange correlation energy functional that depends solely on the electron density at each point of space. The LDA can be easily applied using plane waves with periodic boundary conditions. In this case the exchange correlation energy is calculated as follows:

$$E_{xc}^{LDA}[n] = \int n(\vec{r})\varepsilon_{xc}(n)d^3r \quad (7)$$

2.2 Methods for band structure calculation

In this section, we will discuss the theoretical background behind the electronic band structure calculations we applied to monolayers WS_2, graphene and WS_2/Graphene heterostructures. At first, the calculation of ground state based on DFT uses some simplifications and approximations in order to handle the problem of the infinite number of interacting electrons moving in the static field of an infinite number of ions. The solution of the Schrödinger equation at zero potential is a plane wave. The electrons far from the nuclei behave as free particles and can be represented by plane waves. The electrons close to the nucleus behave as in a free atom and hence, atomic like functions can be used to represent them. The system with electron-electron interactions can be mapped to a non-interacting electron system, and an infinite solid bulk may be considered periodic. The ions in a perfect crystal are arranged in a regular periodic way. Therefore, the external potential felt by the electrons will also be periodic, the period is the same as the length of the unit cell (L).

In one dimension, the external potential on an electron at position r can be expressed as V(r) = V(r + L), which is the condition for the use of Bloch's theorem. With the use of this theorem it is possible to express the wave functions of the infinite crystal in terms of wave functions at reciprocal space vectors of a Bravais lattice. Bloch's theorem uses the periodicity of a crystal to reduce the infinite number of electron wave functions to be calculated, to simply the number of electrons in the unit cell of the crystal. The wave function is written as the product of a cell periodic part and a wave-like part as:

$$\Psi_i(\vec{r}) = e^{i\vec{k}\vec{r}} f_i(\vec{r}) \quad (8)$$

where $f_i(\vec{r})$ a periodic function with the periodicity of the unit cell and k is the k-point that refers to all the values in the first Brillouin zone.

$$f_i(\vec{r}) = \sum_G c_i G e^{i\vec{G}\vec{r}} \quad (9)$$

The first Brillouin zone is the primitive cell (PC) in the reciprocal space, and it is given by the volume surrounded by the surfaces with the same distance from one element

point of the lattice and its neighbors. The reciprocal space in solid-state physics stands for the array of reciprocal lattices. The $\vec{G}$ are the reciprocal lattice vectors which are defined by $G = \frac{2\pi m}{L}$.

Therefore, each electronic wavefunction is written as a sum of plane waves.

$$\Psi_\iota(\vec{r}) = \sum_G c_{i,k+G} e^{i(\vec{k}+\vec{G})\vec{r}} \quad (10)$$

The electronic wavefunctions at each k-point are now expressed in terms of a discrete plane wave basis set. In principle, this Fourier serie is infinite. However, the coefficients for the plane waves $c_{i,\vec{k}+\vec{G}}$ each have a kinetic energy $\frac{\hbar^2(|\vec{k}+\vec{G}|)^2}{2m}$. The plane waves with a smaller kinetic energy typically have a more important role than those with a very high kinetic energy.

So, this introduction of plane wave energy cut off reduces the basis set to a finite size. According to these in this thesis we use plane wave method for electronic band structure calculations. This means that the wave functions are expanded in plane waves and that:

$$\frac{|G+k|^2}{2} < E_{cut} \quad (11)$$

where E_{cut} is the energy plane wave cutoff. In this work $E_{cut} = 600eV$**.**

As we said before, with the Bloch's theorem we can write the electron wave function as a part of a plane wave like and a periodic function as we can see in the equation (8). So, one of the important parameters in this study is the number of k-points. That way all the physical properties in the system are periodic functions of the eigenstates of the $\vec{k}$ vector. We only need to consider $\vec{k}$ vectors inside the primitive unit cell of the reciprocal lattice of the system, which is called Brillouin zone. For example, if we want to solve the Schrödinger's equation for a many body problem in one dimension, we just have to take the k points that are in the range between $-\frac{\pi}{a} \leq k \leq \frac{\pi}{a}$ where a is the lattice constant. In the next figure 2.1, we can see the graphical representation of the k points for the first Brillouin zone for the 2D hexagonal Bravais lattice which is used in our thesis:

Figure 2.1

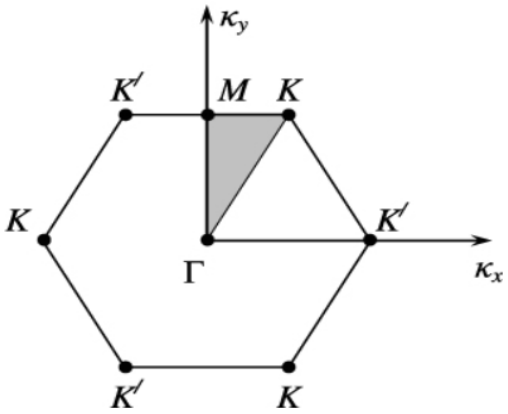

Figure 2.1: First Brillouin zone for 2D hexagonal Bravais lattice.

So, the Brillouin zone sampling[26] is defined with the expression kpts = (N1, N2, N3) where N1, N2 and N3 are positive integers. This will sample the Brillouin zone with a regular grid of N1*N2*N3 k-points. In this work after investigation we determine for all electronic band structure calculations to set kpts = (4, 4, 1). So far, we have described the theory behind the electronic band structure calculation in PC. However, for investigating the electronic band structure for WS_2/graphene heterostructures we need to build first the supercell (SC) for WS_2 and graphene. For this reason, we make appropriate SC in which Bloch's theory may be applied to periodic structures such as monolayers. A SC consists of the vectors that define the cell that can be repeated in three dimensions and produces the required crystal structure and also the atom positions in the cell. At this point, it is important to explore and understand the whole picture about the electronic band structure for SC. Due to the many electrons in the unit cell, the electronic band structure of a SC is complicated. For that reason, we follow the method for unfolding the band structure of the SC to the one of the PC. According to these, we will give below an overview of the theory of electronic band structure unfolding for SC calculations. The basis vectors of the SC and PC satisfy:

$$\vec{A} = M * \vec{a},$$

or

$$\begin{pmatrix} \vec{A}_1 \\ \vec{A}_2 \\ \vec{A}_3 \end{pmatrix} = \begin{pmatrix} m_{11} & m_{12} & m_{13} \\ m_{21} & m_{22} & m_{23} \\ m_{31} & m_{32} & m_{33} \end{pmatrix} * \begin{pmatrix} \vec{a}_1 \\ \vec{a}_2 \\ \vec{a}_3 \end{pmatrix}, \quad m_{ij} \in \mathbb{Z} \quad (12)$$

where $\vec{A}$ and $\vec{a}$ are matrices with the cell basis vectors as rows and M the transformation matrix. Following the convention adopted above we give a relation similar to Eq. (12) which the two reciprocal basis vectors $\vec{B}_i = \left(\frac{2\pi}{V_{SC}}\right) * \left(\vec{A}_j x \vec{A}_k\right)$ and $\vec{b}_i = \left(\frac{2\pi}{u_{PC}}\right) * \left(\vec{a}_j x \vec{a}_k\right)$:

$$\vec{B} = M^{-1} * \vec{b},$$

or

$$\begin{pmatrix} \vec{B}_1 \\ \vec{B}_2 \\ \vec{B}_3 \end{pmatrix} = M^{-1} * \begin{pmatrix} \vec{b}_1 \\ \vec{b}_2 \\ \vec{b}_3 \end{pmatrix}, \quad (13)$$

where u_{PC} and V_{SC} the volumes of the PC and SC unit cells respectively which are related by $V_{SC} = u_{PC} * \det(M)$. Now, given a wave vector $\vec{k}$ in primitive Brillouin zone (PBZ) it is said to fold into a wave vector $\vec{K}$ in supercell Brillouin zone (SBZ) if there exists a reciprocal lattice vector $\vec{G}$ (in the SBZ) such that:

$$\vec{K} = \vec{k} - \vec{G} \quad (14)$$

Conversely, a wave vector $\vec{K}$ unfolds into $\vec{k}_i \in$ PBZ

$$\vec{k} = \vec{K} + \vec{G} \quad (15)$$

These equations (14) and (15) summarize the very principle of folding and unfolding of states. The vectors $\vec{K}$ and $\vec{G}$ in equation (14) are unique for a given $\vec{k}$, which means that a given wave vector $\vec{k} \in$ PBZ is mapped precisely into a single wave vector $\vec{K} \in$ SBZ (folding). In contrast, equation (15) shows that a given wave vector $\vec{K}$ can be obtained from a number $N_{\vec{K}} = \det M$ of different $(\vec{k}_i, \vec{G}_i)$ pairs (unfolding). According to these the electronic structure calculation methods can be applied to a periodic solid using either a PC or a SC representation. By solving the Schrödinger equation of the electronic system, we can obtain both the eigenvectors $|\vec{k}n\rangle$ in PC and $|\vec{K}m\rangle$ in SC (where n and m stand for band indices) and the dispersion relations $E(\vec{k})$ and $E(\vec{K})$, which are well-defined quantities in both representations. In this direction, the basic idea of an unfolding procedure is to recover, from the SC calculation alone, either the PC eigenvectors $|\vec{k}n\rangle$ and their contributions to the SC eigenstates $|\vec{K}m\rangle$, or the $E(\vec{k})$ picture from the often complicated $E(\vec{K})$. The basic relation which has a crucial role in the unfolding method is the spectral function of the PC calculation starting from eigenvalues and eigenfunctions of the SC one. Spectral function can be presented as follows:

$$A(\vec{k}, E) = \sum_m P_{\vec{K}m}(\vec{k}) \delta(E_{\vec{K}m} - E) \quad (16)$$

where $P_{\vec{K}m}(\vec{k})$ are the spectral weights defined by:

$$P_{\vec{K}m}(\vec{k}) = \sum_n |\langle \vec{K}m | \vec{k}n \rangle|^2$$

This quantity represents the probability of finding a set of PC states $|\vec{k}n\rangle$ contributing to the SC state $|\vec{K}m\rangle$ which give information about how much of the amount of Bloch character $|\vec{k}n\rangle$ is preserved in $|\vec{K}m\rangle$[27][28][29].

2.3 Theoretical approximation methods for excitons

After the analysis of the theory for electronic structure calculations in this work we will also study optical excitations in monolayer of WS_2 through DFT calculations. In our thesis, we followed two approximation methods in order to calculate the dynamical dielectric function for excitation effects, which are the Random Phase Approximation (RPA) and Bethe-Salpeter Equation (BSE). For this purpose, it is important in this section to present an overview of RPA and BSE methods respectively.

The RPA[25][30][31] is a non-perturbative method which accounts for the weak screened Coulomb interaction and used for describing the dynamic linear electronic response of many-electron systems. RPA uses local field and electrons are assumed to respond only to the total electric potential $V_{tot}(r)$ which is the sum of the external perturbing potential $V_{ext}(r)$ and a screening potential $V_{sc}(r)$.

$$V_{tot}(r) = V_{ext}(r) + V_{sc}(r) \quad (17)$$

In the RPA, the key quantity is the non-interacting density response function χ^0 which describes the change of the density δn_{n-i} if the external potential undergoes a small change δV_{tot} according to the relation (18).

$$\delta n_{n-i} = \chi^0 \delta V_{tot} \quad (18),$$

where χ^0 is the polarizability of the system in reciprocal space derived by Adler [32] and Wiser [33] and is written as:

$$\chi^0_{GG'}(q,\omega) = \frac{1}{\Omega}\sum_k^{BZ}\sum_{n,n'} \frac{f_{nk}-f_{n'k+q}}{\omega+\varepsilon_{nk}-\varepsilon_{n'k+q}+i\eta} \langle\psi_{nk}|e^{-i(q+G)*r}|\psi_{n'k+q}\rangle_{\Omega_{cell}} \langle\psi_{nk}|e^{i(q+G')*r'}|\psi_{n'k+q}\rangle_{\Omega_{cell}} \quad (19)$$

where ε_{nk} and ψ_{nk} are the eigenvalue and eigen wavefunction, which is normalized to 1 in the crystal volume $\Omega = \Omega cell * N_k$ and q stands for the Bloch vector of the incident wave and G(G′) are reciprocal lattice vectors. The sum of occupation f_{nk} should be the total number of electrons in the crystal, satisfying

$$\sum_{nk} f_{nk} = N_k N \quad (20)$$

where N is the number of electrons in a single unit cell and N_k is the number of unit cells k-points.

The external perturbing potential is assumed to oscillate at a single frequency ω, so that the model yields via a self-consistent field (SCF) method[34] a dynamic dielectric function denoted by $\varepsilon^{RPA}_{GG'}(q,\omega)$ given as:

$$\varepsilon^{RPA}_{GG'}(q,\omega) = \delta_{GG'} - \frac{4\pi}{|q+G|^2}\chi^0_{GG'}(q,\omega) \quad (21)$$

and from that the macroscopic dielectric function is defined by

$$\varepsilon_M(q,\omega) = \frac{1}{\varepsilon_{00}^{-1}(q,\omega)} \quad (22)$$

As a result, the optical absorption spectrum (ABS) is obtained through

$$\mathrm{ABS} = \mathrm{Im}\varepsilon_M(q \to 0,\omega) \quad (23)$$

After we presented the RPA, we will discuss the BSE which is the second theoretical approximation method (for excitons) which we followed. BSE is an object which calculates optical and dielectric properties of material systems including the electron-hole interaction. The BSE has been successfully applied to describe two-particle excitations and represents also a powerful tool to deal with excitation energies like absorption spectra. In this framework, as we understand the BSE calculation is the second stage after DFT. The first stage starts with perform DFT calculation which gives a ground state structure of the system, by solving the Kohn-Sham (KS) equations in LDA. In order to get improved response functions and describe correctly the important excitonic effects we solve the BSE for the polarizability. This leads in general to excellent absorption spectra[70]. In practice, the BSE can be solved by diagonalizing a two-particle excitonic Hamiltonian which moreover provides information about the excitonic eigenstates and eigenvalues. In transition space and using the only-resonant approximation it is given as:

$$H^{eff}A^{\lambda} = E^{\lambda}A^{\lambda} \quad (24)$$

where A^{λ}, E^{λ} are the eigenvectors and eigenvalues of the two-particle Hamiltonian. In practice we evaluate everything in frequency domain, reciprocal space and transitions basis. The excitonic Hamiltonian reads:

$$H^{eff}_{uu'cc'kk'} = (\varepsilon_{ck} - \varepsilon_{uk})\delta_{uu'}\delta_{cc'}\delta_{kk'} + \langle uck|\bar{u}|u'c'k'\rangle - \langle uck|W|u'c'k'\rangle \quad (25)$$

where uu', cc', kk' indexes of valence band, conduction band and k-vector, respectively and ε_{ck} , ε_{uk} are quasi-particle energies.

The term $\bar{u}$ is the Coulomb potential without the long-range part and describes the electron-hole exchange:

$$\langle uck|\bar{u}|u'c'k'\rangle = \frac{4\pi}{\Omega}\sum_{G\neq 0}\frac{1}{|G|^2}\langle ck|e^{iG*r}|uk\rangle\langle u'k'|e^{-iG*r}|c'k'\rangle \quad (26)$$

and W is the screened Coulomb electron-hole interaction part given as:

$$\langle uck|W|u'c'k'\rangle = -\frac{4\pi}{\Omega}\sum_{GG'}\frac{\varepsilon^{-1}_{GG'}(q)}{|q+G|^2}\langle ck|e^{i(q+G)*r}|c'k'\rangle\langle u'k'|e^{-i(q+G)*r}|uk\rangle\,\delta_{q,k-k'} \quad (27)$$

Generally, the goal of BSE is to find a value for the macroscopic dielectric tion $\varepsilon_M(\omega)$ which is directly related with some measurable quantity. The absorption spectrum, is given by the imaginary part of $\varepsilon_M(\omega)$. If we only consider the resonant part of the excitonic Hamiltonian, we permit only positive frequency transitions to mix, the macroscopic dielectric function is given by

$$\varepsilon_{M(\omega)} = 1 - \lim_{q\to 0} u_0(q) \sum_\lambda \frac{\left|\sum_{(uc)} \langle u|e^{-iq*r}|c\rangle A_\lambda^{(uc)}\right|^2}{E_\lambda - \omega - i\eta} \quad (28)$$

Good agreement between theory and experiment can only be achieved by taking into account the electron-hole interaction and the Bethe-Salpeter gives a very successful calculation of ABS.

However, in this case where we study 2D materials, the W which is the screening Coulomb interaction plays a fundamental role in the BSE. For this reason, the W requires a special treatment in order to decouple and eliminate the screening from layers in periodic images to better describing the excitonic effects in 2D materials. The solution comes with use of a truncated Coulomb interaction[71] which implanted in BSE (BSE-truncated) with screened interaction W gives:

$$W_{00}(q = 0) = \frac{1}{\Omega_\Gamma} \int dq u_c(q) \left[1 + q * \nabla_q \varepsilon_{00}^{-1}(q)|_{q=0}\right] \quad (29)$$

where Ω_Γ is a small volume containing q = 0 and $u_c(q) = \frac{4\pi R_c}{|q|}$ is the truncated Coulomb interaction which effect to eliminated the interlayer interactions.

2.4 Computational details

In the last section of this chapter we will give some additional computational details we applied on thesis, including calculation parameters.

Monolayers of WS_2, Graphene and heterostructures of WS_2/Graphene are investigated using DFT, where the LDA exchange-correlation functional was used and the systems were modelled using the Atomic Simulation Environment (ASE) module.[35] The calculations were performed using the Grid-based Projector-Augmented Wave (GPAW) module[36], which is a DFT python code based on the Projector-Augmented Wave (PAW) method. The wave functions are described with Plane-Waves (PW) mode. We applied the parameter "mode = PW(600)" which means the plane-wave energy cut off is 600eV and for all calculations. In the monolayer WS_2 and all of heterostructures which include already tungsten (W), we defined the parameter "setups = {'W': '6'}" which means for each W we have six valence electrons. The optimal number of k-points in Brillouin-zone chosen for all of the systems is (k_x, k_y, k_z) = (4, 4, 1) which gives a well-converged energy. Additionally, the selection for the number of electronic bands (which was done with the parameter "nbands") depended on the number of atoms and was at least equal to 50% more than the number of atomic orbitals. In this work for each calculation we added more unoccupied bands for improved convergence. In order to control the smearing of the occupation numbers of electronic states, we set the parameter "occupations = FermiDirac(0.01)" which means the width

of the electronic levels is 0.01eV according to the Fermi-Dirac distribution. To conclude, for all structures we also added 8Å vacuum of unit cell in the z-axis direction to avoid any convergence problems in simulation box.

Chapter 3

WS_2 monolayer and Graphene

In order to achieve the purpose of this thesis which is the study of WS_2/graphene heterostructures, it is necessary to define and examine the WS_2 monolayer and graphene separately. In this chapter, we will present the foundations of our thesis which is a WS_2 monolayer and graphene, two materials which belong to the family of 2D materials. We examined a WS_2 monolayer which was constructed from a primitive cell (PC) consisting of three atoms (W, 2 S) and a 3x3 WS_2 supercell (SC) which consists of twenty-seven atoms (9 W, 18 S). Furthermore, we investigated graphene which was constructed of a PC consisting of two atoms (2 C) and a 4x4 graphene supercell (SC) which consists of thirty-two atoms (32 C). We will discuss shortly the characteristics for each one and next we will analyze the results we obtained from DFT calculations for the atomic structure and the electronic band structure in these 2D materials. The purpose of these DFT calculations for WS_2 monolayer and graphene is to find the optimal structural parameters which minimize the total ground state energy. We present reliable structural and electronical properties which are agree with experimental results.

3.1 WS_2 monolayer

WS_2 monolayer is a material in the TMDs family. As a semiconductor, it has a direct band gap 2.1eV[37][38] that offers significant optoelectronic properties[18] which are promising for use in electronics. WS_2 monolayer is a layered material with sheets consisting of a layer of tungsten atoms sandwiched between two layers of sulfur atoms in a trigonal prismatic coordination as seen in Figure 3.1. In this section, we examine and discuss the theoretical results from DFT calculations for the atomic and electronic structure of monolayer WS_2 and compare with the current experimental works.

Figure 3.1

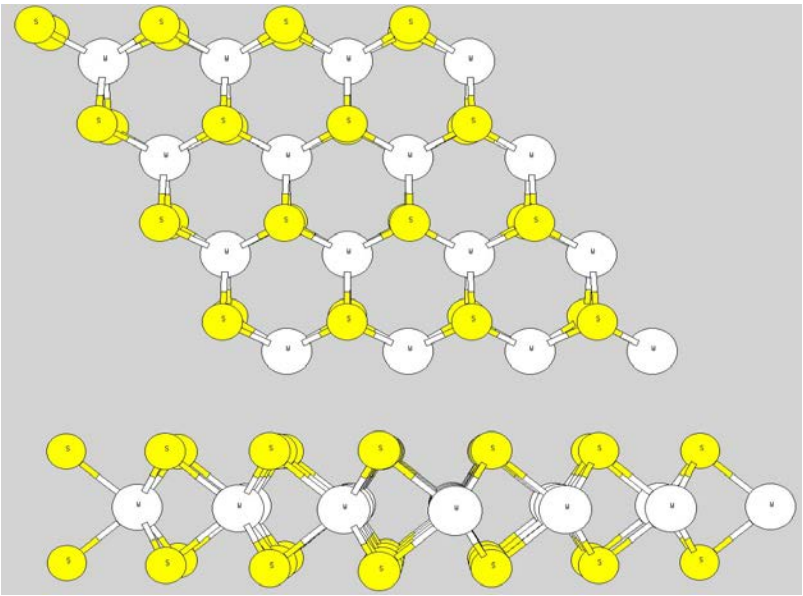

Figure 3.1: The atomic structure of WS_2 showing the trigonal prismatic coordination as well as the sandwiched layered structure of the material.

3.1.1 Structure of WS_2 monolayer

In this subsection, we show the structure of WS_2 monolayer which is a PC consisting of 3 atoms (W, S, S) as we see in Figure 3.2. We performed DFT calculations in order to find the optimal structural parameters as well as the minimum total energy ground state of the system. As we said, WS_2 monolayer has hexagonal structure in trigonal prismatic coordination with space group P63/mmc. The geometry is defined by the lattice vectors $\mathbf{a_1}$, $\mathbf{a_2}$, $\mathbf{a_3}$ and the atom position vectors R_W, R_S, R_S within the unit cell. They can be defined in various different but equivalent ways. In this work, we use the following configuration for the lattice vectors:

$$\mathbf{a_1} = a\,(-1/2, \sqrt{3}/2, 0),\ \mathbf{a_2} = a\,(1, 0, 0),\ \mathbf{a_3} = c\,(0, 0, 1)$$

where a is the lattice constant, c is the parameter of hexagonal lattice

Now, the position vectors for tungsten (W) and sulfurs (S):

$$R_W = 1/3\ \mathbf{a}_1 + 2/3\ \mathbf{a}_2 + 1/4\ \mathbf{a}_3$$

$$R_S = 2/3\ \mathbf{a}_1 + 1/3\ \mathbf{a}_2 + (1\text{-}u)\ \mathbf{a}_3$$

$$R_S = 2/3\ \mathbf{a}_1 + 1/3\ \mathbf{a}_2 + (u\text{-}1/2)\ \mathbf{a}_3$$

where u is the parameter which determines the distance between sulfurs. The distance $d_{s\text{-}s}$ between sulfurs for WS_2:

$$d_{s\text{-}s} / 2 = (3/4 - u) * c \quad (30)$$

Figure 3.2

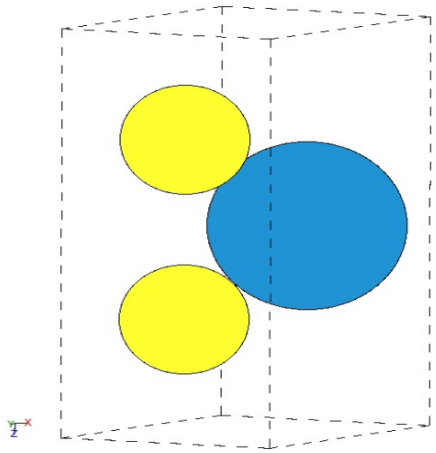

Figure 3.2: The unit cell of WS_2 monolayer consists of three atoms W, S, S.

According to the above lattice vectors $\mathbf{a_1}$, $\mathbf{a_2}$, $\mathbf{a_3}$ and the atom position vectors R within the unit cell, we performed some iterations with DFT and calculated the total energy of system around of lattice constant a=3.153Å[37][39] and parameter u=0.618 (d_{s-s} = 3.148Å). We kept the parameter c=12Å constant.

The iterations started with lattice constant a of 3.11Å to 3.19Å with step 0.01Å and for each value of the calculation the total energy is shown Table.1.

Table.1

Energy (eV)	Lattice constant (Å)
-24.277	3.11
-24.286	3.12
-24.292	3.13
-24.295	3.14
-24.296	**3.15**
-24.294	3.16
-24.290	3.17
-24.283	3.18
-24.274	3.19

The energy curve E (eV) (axis -y) as a function of lattice constant a (Å) (axis -x) was fitted to a second degree polynomial of the form:

$$y = ax^2 + bx + c \quad (31)$$

Figure 3.3

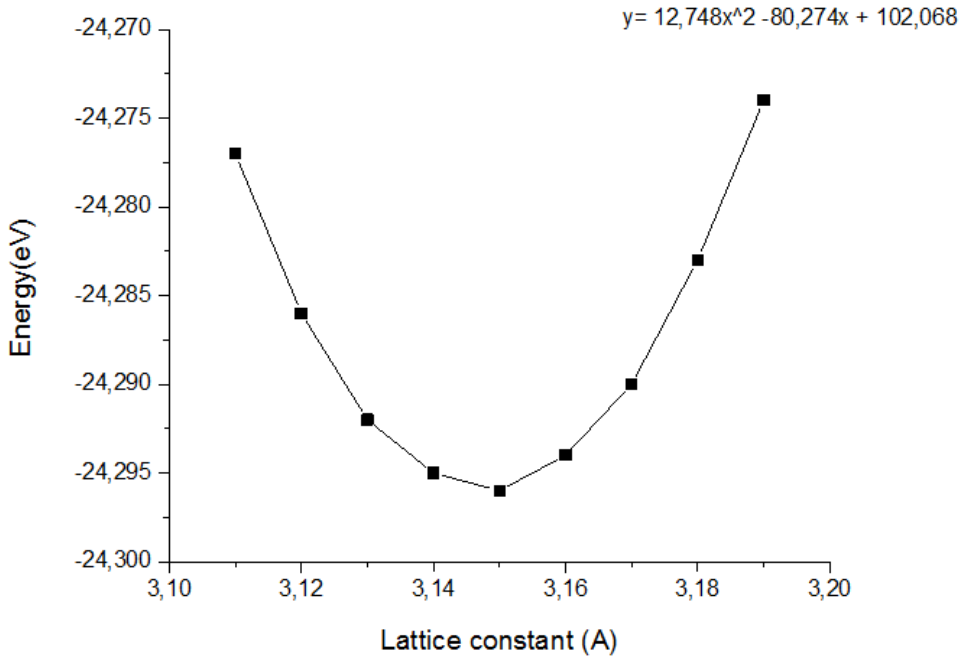

Figure 3.3: The energy curve E (eV) as a function of lattice constant a (Å) of WS_2 monolayer.

Determining the minimum,

dy/dx = 2ax + b=0 => x= - b/(2a) =>x=3.148 we find **a=3.148Å, E_{min}=-24.296eV**

Furthermore, we followed the same procedure and performed some iterations around of parameter u=0.618 (d_{s-s}=3.148Å) while keeping lattice constant a=3.148Å and c=12Å stable. The iterations began with u parameter of 0.615 to 0.621 with step 0.001 and done for each value the calculation of total energy as we seen in Table.2.

Table.2

Energy (eV)	Parameter u
-24.255	0.615
-24.274	0.616
-24.287	0.617
-24.295	0.618
-24.296	**0.619**
-24.292	0.620
-24.281	0.621

The energy curve E (eV) (axis -y) as a function of parameter u (axis -x) is fitted with a second degree polynomial of the form (31).

Figure 3.4

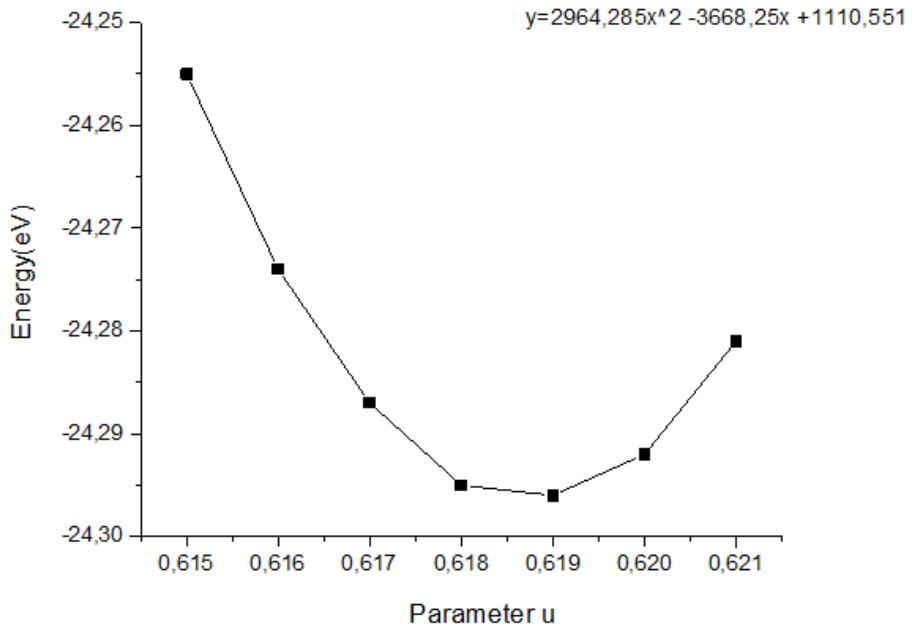

Figure 3.4: The energy curve E (eV) as a function of parameter u of WS_2 monolayer. Determining the minimum,

$dy/dx = 2ax + b=0 \Rightarrow x= - b/(2a) \Rightarrow x=0.619$

we find **$u=0.619$ (d_{s-s}=3.144Å), E_{min}=-24.296eV**

According to these results, were determined as the optimized unit cell lattice parameters a=3.148Å, u=0.619 (d_{s-s}=3.144Å), c=12Å for the WS_2 monolayer. Percentage error is only 0.158% with the experimental value of lattice constant a=3.153Å[37] for the WS_2 bulk crystal and that means we have reliable results for the description of the structure of this material.

3.1.2 Electronic band structure of WS_2 monolayer

After a review of the structure of the WS_2 monolayer and after finding the optimized structural parameters, we discuss its electronic structure. The band structure of WS_2 monolayer and its isoelectronic compounds of the group six TMD family, is distinctly different from that of graphene. The indirect to direct crossover in single layer WS_2 results from local shift of valence band hills and conduction band valleys in the Brillouin zone[41]-[47]. The conduction band minimum (CBM) and valence band maximum (VBM) coincide at the K point, making them direct gap semiconductor. In this subsection, this behavior is predicted by DFT calculations and is in agreement with photoemission experiments on WS_2 single layer[48]. Based on the results for the structure of WS_2 monolayer, with optimized unit cell lattice parameters are a=3.148Å, u=0.619 (d_{s-s} = 3.144Å), c=12Å, we perform DFT calculations for the electronic band structure. The basis vectors of the corresponding reciprocal lattice are

$$\mathbf{b_1} = (2\pi/a)*(0, -\sqrt{\frac{1}{3}}, 0), \mathbf{b_2} = (2\pi/a)*(1, \sqrt{\frac{1}{3}}, 0)$$

and the Brillouin zone for the 2D crystal is a hexagon as seen in Figure 3.5.

Figure 3.5

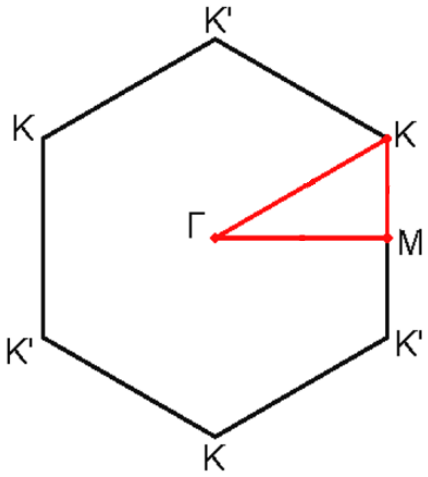

Figure 3.5: The 2D Brillouin zone of WS_2.

In this electronic band structure calculation of WS_2 monolayer we selected the M-K-G path in the Brillouin zone to represented the result as shown below.

Figure 3.6

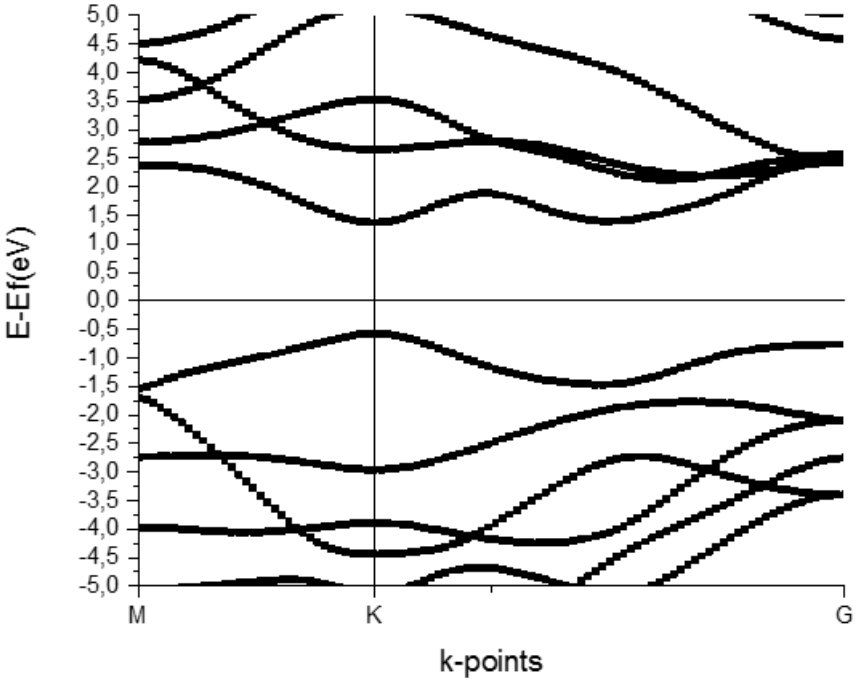

Figure 3.6: Bandstructure of WS_2 monolayer.

The electronic band structure for WS_2 monolayer on the above diagram was calculated within the LDA approximation with 1.945eV direct band gap in K-point and Fermi level was set to zero ($E-E_{fermi}$ = 0eV) with Fermi energy E_{fermi} = -1.080eV. We observed that the PW mode in LDA gives very good description of the electronic structure, close to the experimental 2.1eV[37][38][40] band gap.

3.1.3 Structure of WS_2 supercell

In order to achieve the purpose of this thesis which is the study of WS_2/graphene heterostructures, it is necessary to define supercells (SCs) of WS_2 monolayer. This plays a crucial role in the structure and stability of WS_2/graphene heterostructure. The SCs consist of PC with the same lattice vectors $\mathbf{a_1}$, $\mathbf{a_2}$, $\mathbf{a_3}$ as in the subsection 3.1.1 that are repeated in two dimensions (x and y) and produce the required monolayer structure and the atom positions in the (SC). We produced and studied the 3x3 supercell (SC) of WS_2 monolayer which consists of 27 atoms (9 W, 18 S) as we see in Figure 3.7. We performed DFT calculations as in section 3.1.1 to find the optimal structural parameters as well as to minimum total ground state energy of system.

Figure 3.7

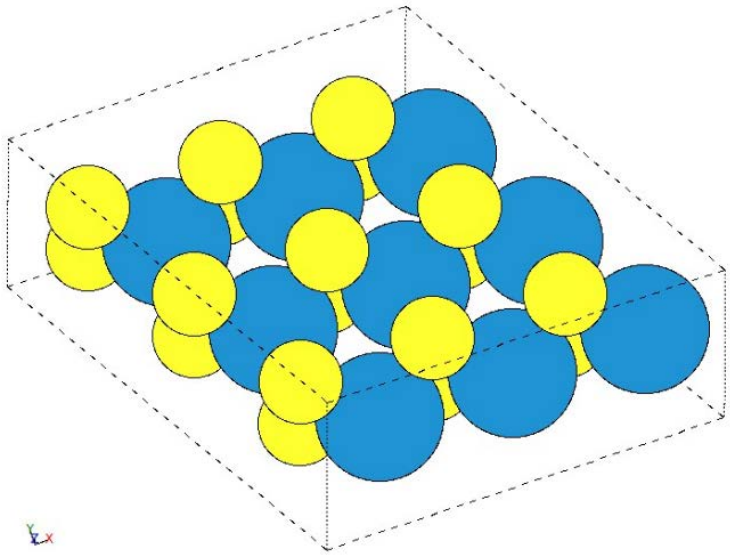

Figure 3.7: 3x3 supercell of WS_2 monolayer consisting of 27 atoms (9 W, 18 S).

We performed some iterations with DFT for calculating the total energy of system around of lattice constant a=9.444Å (3x3.148Å) and parameter u=0.618 (d_{s-s} = 3.148Å) which as we said determines the distance between sulfurs. We kept the parameter c=12Å stable. The iterations started with SC lattice constant a of 9.40Å to 9.48Å with step 0.01Å for the calculation of the total energy as we see in Table.3.

Table.3

Energy (eV)	Lattice constant (Å)
-218.820	9.40
-218.830	9.41
-218.838	9.42
-218.842	9.43
-218.844	**9.44**
-218.843	9.45
-218.839	9.46
-218.833	9.47
-218.824	9.48

The energy curve E (eV) (axis -y) as a function of lattice constant a (Å) (axis -x) is fitted with second degree polynomial of the form (31).

Figure 3.8

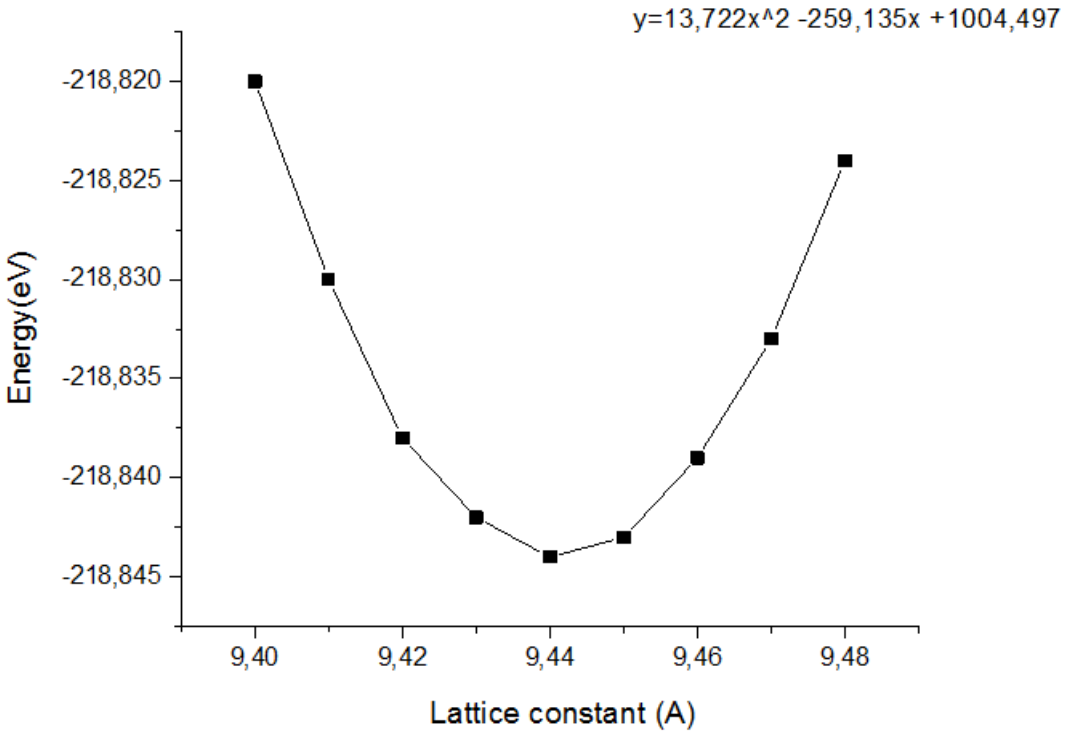

Figure 3.8: The energy curve E (eV) as a function of lattice constant a (Å) of WS_2 supercell.

Determining the minimum,

dy/dx = 2ax + b=0 => x= - b/(2a) =>x=9.442 we find **a=9.442Å, E_{min}=-218.844eV**

Furthermore, we followed the same procedure and performed some iterations around of parameter u=0.618 (d_{s-s}=3.148Å) while keeping lattice constant a=9.442Å and c=12Å stable.

The iterations began with u parameter of 0.615 to 0.621 with step 0.001 and done for each value the calculation of total energy as we seen in Table.4.

Table.4

Energy (eV)	Parameter u
-218.461	0.615
-218.632	0.616
-218.754	0.617
-218.825	0.618
-218.844	**0.619**
-218.808	0.620
-218.715	0.621

The energy curve E (eV) (axis -y) as a function of parameter u (axis -x) is fitted with a second degree polynomial of the form (31).

Figure 3.9

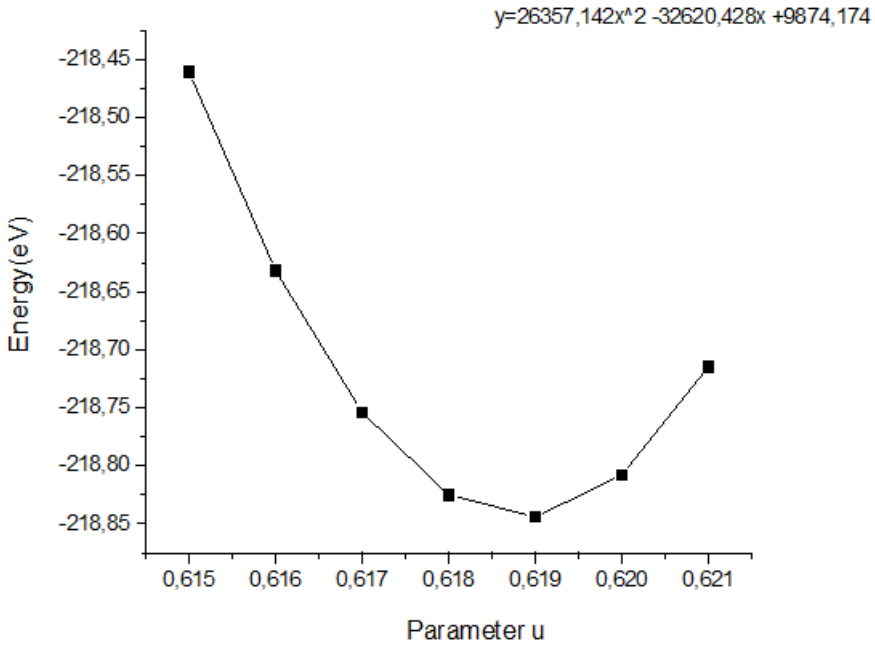

Figure 3.9: The energy curve E (eV) as a function of parameter u of WS_2 supercell.

Determining the minimum,

dy/dx = 2ax + b=0 => x= - b/(2a) =>x=0.619

we find **u=0.619 (d_{s-s} = 3.144Å), E_{min}=-218.844eV**

According to these results, are determined the optimized lattice parameters a=9.442Å, u=0.619 (d_{s-s} = 3.144Å), c=12Å for the 3x3 SC of WS_2 monolayer. We have the same lattice parameters with the PC of 3 atoms of WS_2 monolayer where we discussed in subsection 3.1.1 except for lattice constant a=9.442Å which has a value closely to 3x3.148Å as we expected because of the periodicity of PC by 3 in x and y direction. These results mean we have made successfully built of SC for description of structure in this material.

3.1.4 Electronic band structure of WS_2 supercell

After a review of the structure of 3x3 supercell (SC) of WS_2 monolayer and after we found the optimized structural parameters, we discuss the electronic structure of WS_2 supercell. We expected the conduction band minimum (CBM) and valence band maximum (VBM) to coincide at the K point, giving a direct gap semiconductor. Based on the results of the structure of WS_2 supercell, for the optimized supercell lattice parameters a=9.442Å, u=0.619 (d_{s-s} =3.144Å), c=12Å, we perform DFT calculation for the electronic band structure. The Brillouin zone is a hexagon as we discussed in subsection 3.1.2 (Figure 3.5). In this electronic band structure calculation of WS_2 supercell we selected the M-K-G path in Brillouin zone to represent the result as shown below.

Figure 3.10

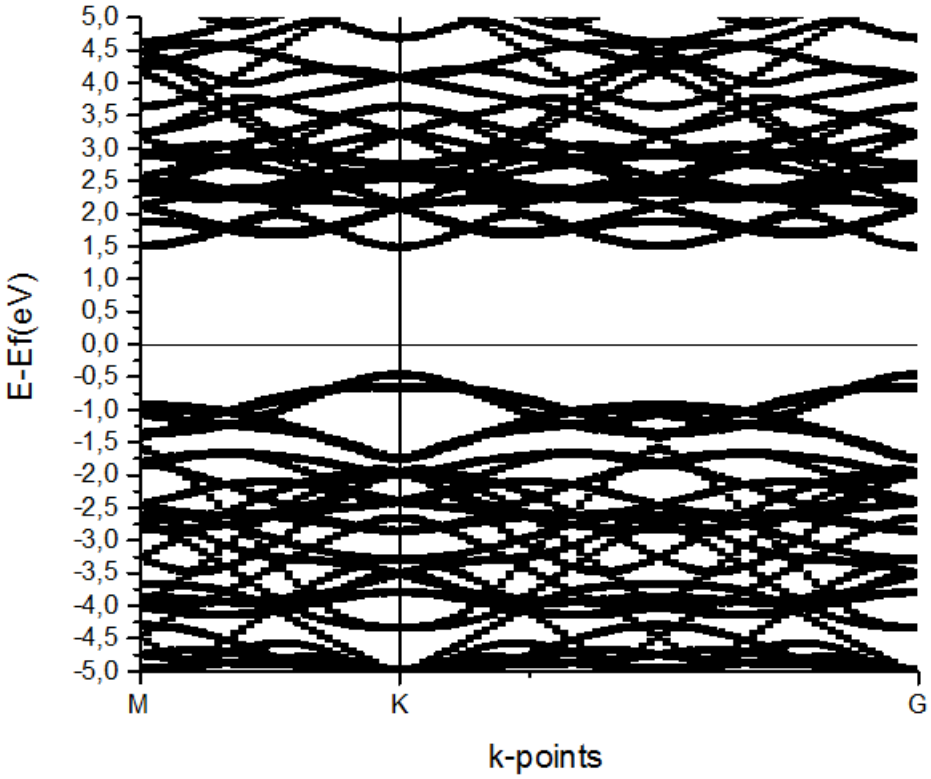

Figure 3.10: Bandstructure of WS_2 supercell.

The electronic band structure for the WS_2 supercell on the above diagram must be exactly the same with WS_2 monolayer, as we discussed in subsection 3.1.2. However, we observe a large number of electronic bands which give a confusing and unrealistic electronic band structure picture for the WS_2 monolayer. The explanation comes from the periodicity of SC (3x3 PC in this case) as well as the large number of valence electrons which of this system.

The quite messy electronic band structure of WS_2 supercells is resolved with the band structure unfolding method. This method described in section 2.2 aims to unfold the band structure of the SC to the PC. For this unfolding electronic band structure calculation of the WS_2 supercell we selected the same M-K-G path in Brillouin zone and the is shown below (Figure 3.11).

Figure 3.11

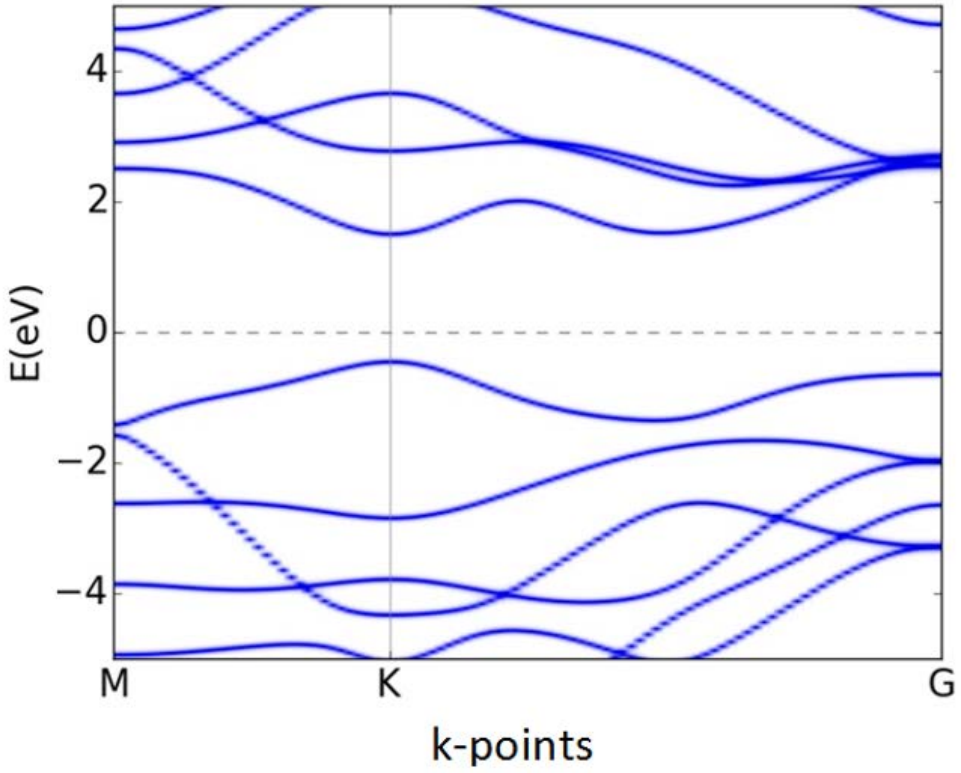

Figure 3.11: Unfolding bandstructure of WS_2 supercell.

As we can see above, is clarified confusing picture for the electronic band structure calculation for the WS_2 supercell. In this electronic band structure diagram, we got 1.949eV direct band gap in K-point and Fermi level was set to zero ($E-E_{fermi} = 0eV$) with Fermi energy E_{fermi} = -1.177eV which is almost the same with the WS_2 monolayer. In conclusion, this method proved a useful tool to produce the real electronic structure picture for WS_2 supercell and also gave reliable results which agree with the PC WS_2 monolayer calculation (Figure 3.6).

3.2 Graphene

Graphene is made of sp^2 hybridized carbon atoms arranged in a hexagonal honeycomb lattice[49][50] as seen in see Figure 3.12. The sp^2 hybridizations between the s orbital and two p orbitals lead to a trigonal planar structure with a formation of σ bond between carbon atoms. Graphene is a semi-metal with a characteristic electronic structure which is band gap free. It exhibits outstanding electronic, optical, mechanical and thermal properties. This makes it interesting for a multitude of applications, such as flexible electronics and to replace rare elements used as transparent conductors, for example in displays[51]. In this section, we will introduce the theoretical results from DFT calculations for the atomic and the electronic structure of graphene and compare them with experimental results.

Figure 3.12

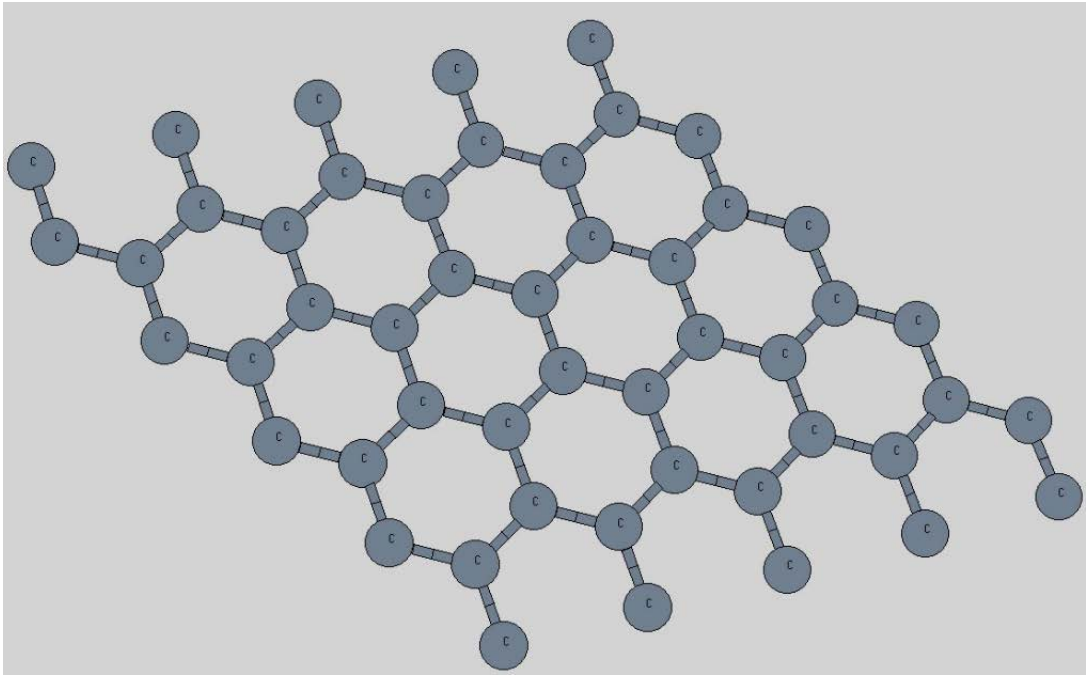

Figure 3.12: Shows the hexagonal structured carbon atoms of monolayer graphene.

3.2.1 Structure of Graphene

In monolayer graphene, three of the four valence electrons hybridize in an sp^2 configuration to form the strong σ bonds while the last electron of the carbon atoms forms the half-filled $2p_z$ orbital normal to the plane of hexagonal carbon lattice, resulting in π covalent bonds. There are three atomic orbitals of sp^2 covalent bonding for each carbon atom, 2s, $2p_x$, and $2p_y$. The strong σ bonds are the main reason for the mechanical strength and structural robustness of the lattice structure in carbon allotropes. Governed by the Pauli principle, these lower energy levels form a deep fully filled valence band. These strong covalent bonds make graphene the thinnest, and yet the strongest material ever measured, being at least five to ten times stronger than steel[54][55].

In this subsection, we build the structure of graphene with a PC consisting of two atoms of carbon (C, C) as seen in Figure 3.13. We performed DFT calculations in order to find the optimal structural parameter which is the lattice constant as well as the minimum total (ground state) energy of system. We define for graphene in cartesian coordinates the real space unit vectors $\mathbf{a_1}$, $\mathbf{a_2}$, $\mathbf{a_3}$ and the atom position vectors R_C within the unit cell:

$$\mathbf{a_1} = a\,(\sqrt{3}/2,\ 1/2,\ 0),\ \mathbf{a_2} = a\,(-\sqrt{3}/2,\ 1/2,\ 0),\ \mathbf{a_3} = c\,(0,\ 0,\ 1)$$

where a is the lattice constant and c is the parameter of hexagonal lattice.

Now the position vectors for two carbons (C):

$$R_C = 0\ \mathbf{a}_1 + 0\ \mathbf{a}_2 + 1/4\ \mathbf{a}_3$$

$$R_C = 1/3\ \mathbf{a}_1 + 2/3\ \mathbf{a}_2 + 1/4\ \mathbf{a}_3$$

Figure 3.13

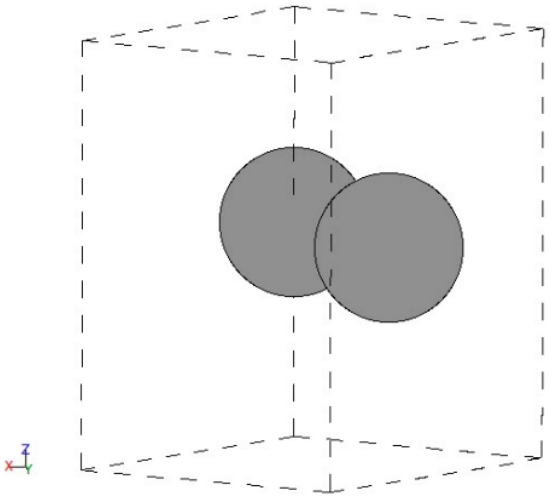

Figure 3.13: Unit cell of graphene consist of two atoms of carbon C.

We performed some iterations with DFT for calculating the total energy of the system around of lattice constant of a = 2.46Å[52] while keeping the parameter c=8Å stable.

The iterations started with lattice constant a of 2.40Å to 2.50Å with step 0.01Å and for each value, the calculation of total energy is presented in Table.5.

Table.5

Energy (eV)	Lattice constant (Å)
-20.136	2.40
-20.157	2.41
-20.173	2.42
-20.183	2.43
-20.189	2.44

-20.190	**2.45**
-20.186	2.46
-20.178	2.47
-20.165	2.48
-20.149	2.49
-20.128	2.50

The energy curve E (eV) (axis -y) as a function of lattice constant a (Å) (axis -x) is fitted with a second degree polynomial of the form (31).

Figure 3.14

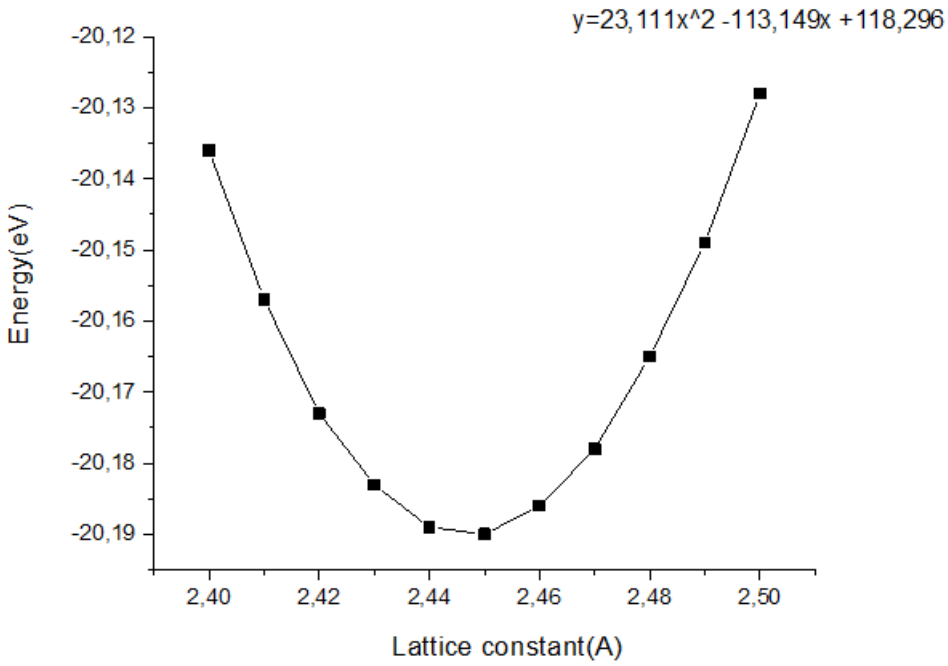

Figure 3.14: The energy curve E (eV) as a function of lattice constant a (Å) of graphene.

Determining the minimum,

dy/dx = 2ax + b=0 => x= - b/(2a) =>x=2.447 we find **a=2.447Å, E_{min}=-20.190eV**

According to these results, the optimized unit cell lattice parameters a=2.447Å and c=8Å for the graphene. We have a percentage error only 0.520% are comparing to the experimental value of the lattice constant 2.46Å[52][53] and that means we have reliable results for the description of the structure of graphene.

3.2.2 Electronic band structure of Graphene

After studying the atomic structure of graphene and having found the optimized lattice constant where the system has minimum total energy, we investigated the electronic structure. Based on modern band structure studies of graphene, the material demonstrates typical properties as a semimetal. The electronic excitations however exhibit a unique linear dispersion with properties resembling to “relativistic” particles. The conduction band and the valence band in pristine graphene meet at a single point around which the wave functions of electrons are described by the Dirac equation, in contrast with conventional 2D systems which a hyperbolic dispersion relation[56]. According to the results for the structure of graphene we set the optimized unit cell lattice parameters a=2,447Å and c=8Å to performed DFT calculations for the electronic band structure. The basis vectors of the corresponding reciprocal lattice are

$$h_1 = 2\pi/\alpha^*(\frac{1}{\sqrt{3}}, 1, 0),\ h_2 = 2\pi/\alpha^*(-\frac{1}{\sqrt{3}}, 1, 0)$$

The Brillouin zone for the graphene is the hexagon seen in Figure 3.15.

Figure 3.15

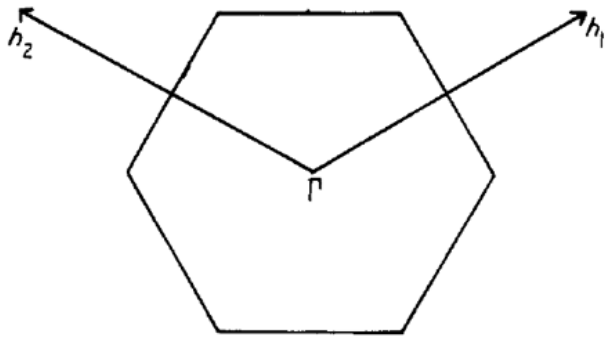

Figure 3.15: The 2D Brillouin zone of graphene.

In this electronic band structure calculation of graphene, we selected the M-K-G path of the Brillouin zone to represent the results, as seen below (Figure 3.16).

Figure 3.16

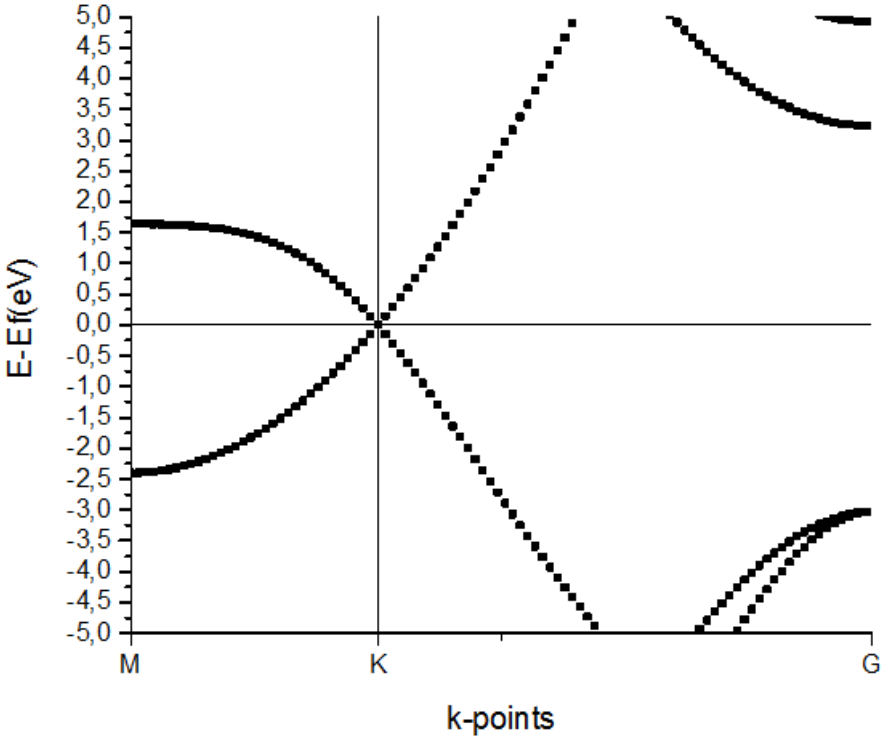

Figure 3.16: Bandstructure of graphene.

The electronic band structure for graphene on the above diagram was calculated by LDA. The results show as zero band gap at the K-point and Fermi level was set to zero ($E-E_{fermi}$ = 0eV) with Fermi energy E_{fermi} = -0.928eV. This band structure description is supported by most existing experimental data.

3.2.3 Structure of Graphene supercell

In this subsection, we define the structure of graphene supercell (SC). The SC consist of PC with the same lattice vectors $\mathbf{a_1}$, $\mathbf{a_2}$, $\mathbf{a_3}$ as in the subsection 3.2.1 that are repeated in two dimensions x and y and produces the required monolayer structure and also the atom positions in the cell. In this case, we produce and study a 4x4 supercell (SC) of graphene which consists of 32 atoms of carbon C as seen in Figure 3.17. We follow the same procedure to perform DFT calculations as in section 3.2.1 to find the optimal structural parameters as well as to minimum total ground state energy of the system.

Figure 3.17

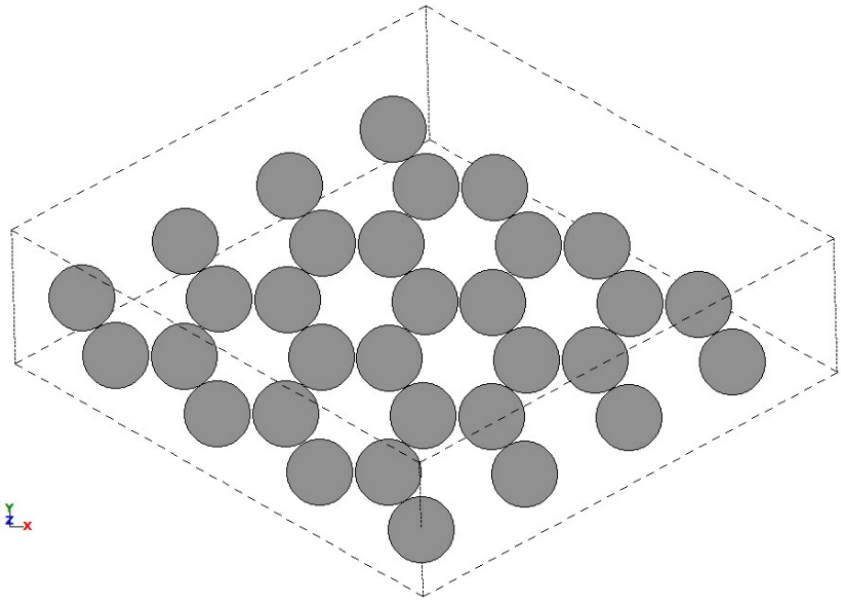

Figure 3.17: 4x4 supercell of graphene consist of 32 atoms of carbon C.

We performed some iterations with DFT for calculating the total energy of the system around the lattice constant a=9.788Å (4x2.447Å) while keeping the parameter c=8Å fixed. The iterations started with a lattice constant of 9.74Å to 9.83Å with step 0.01Å and the total energy is seen in Table.6.

Table.6

Energy (eV)	Lattice constant (Å)
-323.201	9.74
-323.220	9.75
-323.235	9.76
-323.244	9.77
-323.249	9.78
-323.249	**9.79**
-323.246	9.80
-323.236	9.81
-323.223	9.82
-323.204	9.83

The energy curve E (eV) (axis -y) as a function of lattice constant a (Å) (axis -x) is fitted with a second degree polynomial of the form (31).

Figure 3.18

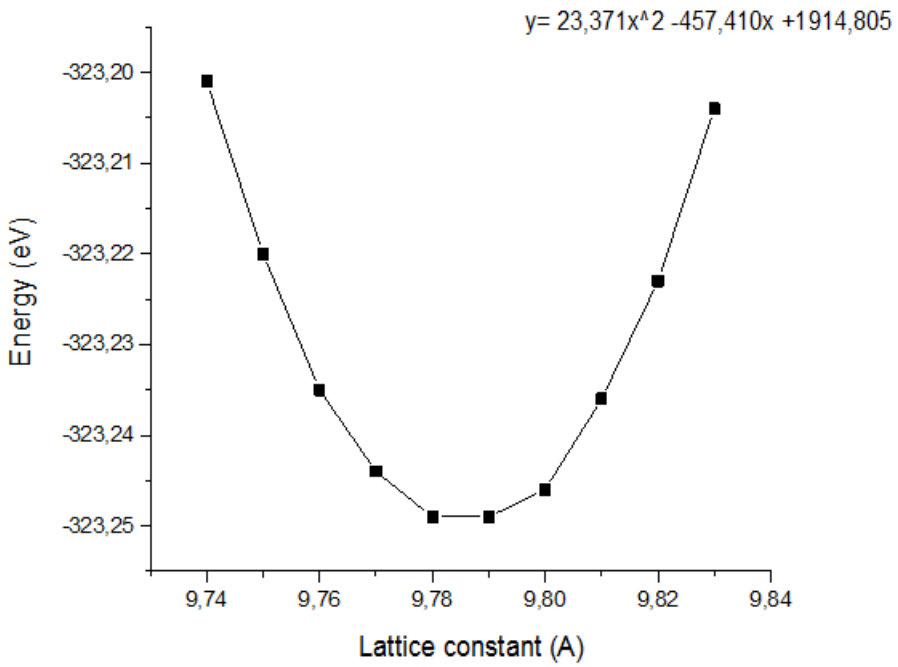

Figure 3.18: The energy curve E (eV) as a function of lattice constant a (Å) of graphene supercell.

Determining the minimum,

dy/dx = 2ax + b=0 => x= - b/(2a) =>x=9.785 we find **a=9.785Å, E_{min}=-323.250eV**

According to these results, the optimized lattice parameters are a=9.785Å, c=8Å for the 4x4 SC of graphene. The value of lattice constant a=9.785Å is close to 4x2.447Å as expected because of the periodicity of PC by 4 in x and y direction. These results mean that we have successfully constructed SC to describe the graphene structure.

3.2.4 Electronic band structure of Graphene supercell

After a review of the structure of 4x4 supercell (SC) of graphene and after we found the optimized structural parameters, we discussed the electronic structure of graphene supercell. The Brillouin zone is a hexagon as we discussed in subsection 3.2.2 (Figure 3.15). We expect the conduction band minimum (CBM) and the valence band maximum (VBM) to meet at a single point K, where the wave functions of electrons are described by the Dirac equation.

Based on the results of the structure of graphene supercell with optimized supercell lattice parameters a=9.785Å and c=8Å we performed DFT calculation for the electronic band structure. In this electronic band structure calculation of graphene

supercell, we selected the M-K-G path in Brillouin zone to represent the result as shown below (Figure 3.19).

Figure 3.19

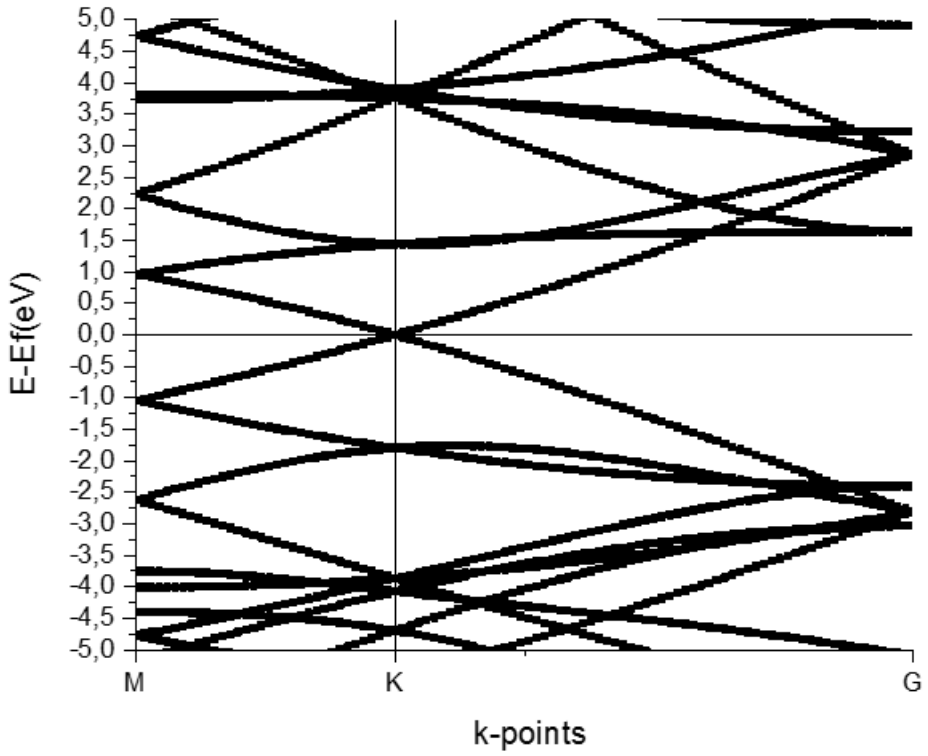

Figure 3.19: Bandstructure of graphene supercell.

The electronic band structure for graphene supercell on the above diagram should must be exactly the same with graphene, as we discussed in subsection 3.2.2. However, we observe many other electronic bands which give a confusing and unrealistic electronic band structure picture for graphene. The explanation comes on from the periodicity of PC (4x4 in this case) as well as the many valence electrons which has this system. Applying the unfolding method described in section 2.2 the result is shown below (Figure 3.20)

Figure 3.20

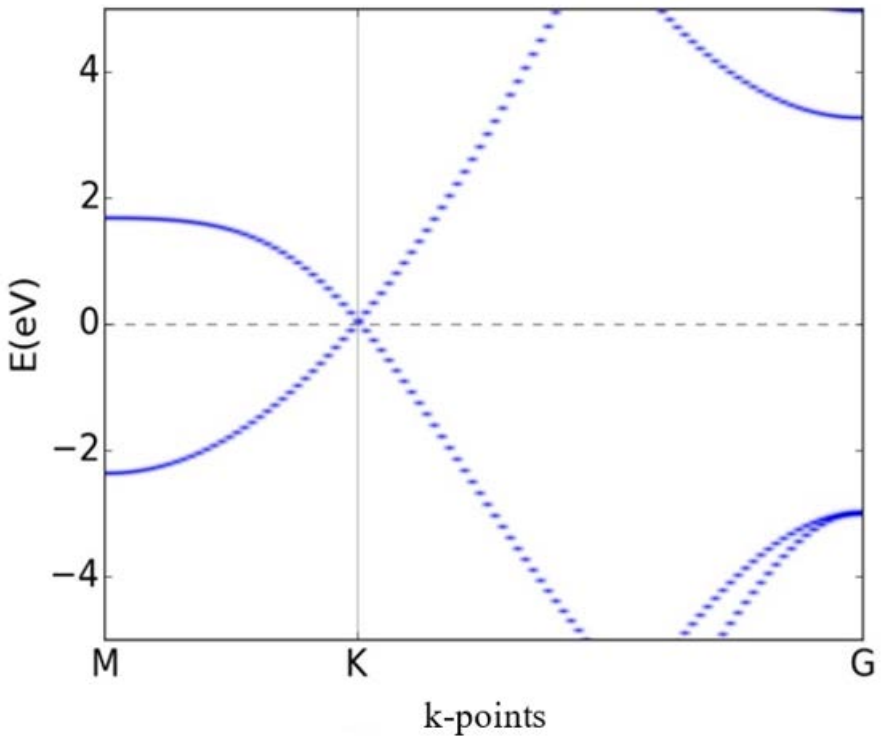

Figure 3.20: Unfolding bandstructure of graphene supercell.

As we can see above, the confused picture is clarified for the electronic band structure for graphene supercell. In this electronic band structure diagram, we got 0eV band gap in K-point and Fermi level was set to zero ($E-E_{fermi}$ = 0eV) with Fermi energy E_{fermi} = -0.926eV which is almost the same with the graphene. In conclusion, this method proved a useful tool to produce the real electronic structure picture for graphene supercell and also gave reliable results which agree with graphene PC. At this point, upon completion of chapter 3 we see that DFT calculations within LDA, describe very well the atomic and electronic structure of WS_2 monolayer and graphene. Moreover, the band structure unfolding method gave us the right information about electronic structure of supercells and will help us to understood the physical meaning of these. With these tools, we move on to the next step to described the WS_2/Graphene heterostructures, which we will discuss in chapter 4.

Chapter 4

WS_2/Graphene heterostructures

The 2D materials, which includes WS_2 monolayer and graphene, can be fabricated into atomically thin films since the intralayer bonding arises from their strong covalent character, while the interlayer interaction is mediated by weak van der Waals (vdW) forces. The weak electron coupling at the interface of vdW heterostructures offers the possibility of combining the intrinsic electronic properties of the individual 2D layers.

In particular, WS_2/Graphene vdW heterostructures are remarkable because of the high carrier mobility[57] and broadband absorption[58] of graphene, as well as the direct bandgap[21][59][61] and extremely strong light matter interactions[62] of monolayer WS_2. For this reason, these unique WS_2/Graphene heterostructures are candidates for many potential applications such as solar photovoltaics. Based on these, in this chapter 4 we will theoretical investigate for WS_2/Graphene heterostructures. We studied two different sizes of supercells (SC) WS_2 (3 × 3)/Graphene (4 × 4), which consists of 59 atoms, and WS_2 (4 × 4)/Graphene (5 × 5), which consists of 98 atoms. We performed DFT calculations for the atomic structure and electronic band structure in these vdW heterostructures. This theoretical investigation has led to a pressing need for a full understanding of the electronic structure as well as to explain the behavior of band alignment of strained WS_2/Graphene vdW heterostructures.

4.1 Heterostructure of WS_2(3x3)/Graphene(4x4)

In this section, we will discuss the SC of WS_2 (3 × 3)/Graphene (4 × 4) heterostructure which is consist of 59 atoms on TW (Top Tungsten) configuration, that means the layers stacked in specific orientation with fifth tungsten (W) atom is over of twelfth carbon (C) atom as we see in Figure 4.1. We performed DFT calculations for the WS_2 (3 × 3)/Graphene (4 × 4) heterostructure to find the optimal structural parameters which minimize the total ground state energy. Based on these theoretical results we will discuss also the lattice mismatch in the supercell and its crucial role in the stability of the heterostructure.

Furthermore, we will examine and discuss the theoretical results from DFT calculations. In the electronic structure of the WS_2 (3 × 3)/Graphene (4 × 4) heterostructure to is examined if the behavior of miss-crossing band alignment of the heterostructure is connected directly with the lattice mismatch. The strain in WS_2 (3 × 3)/Graphene (4 × 4) heterostructure affects dramatically the electronic band structure picture and that is confirmed with our results.

Figure 4.1

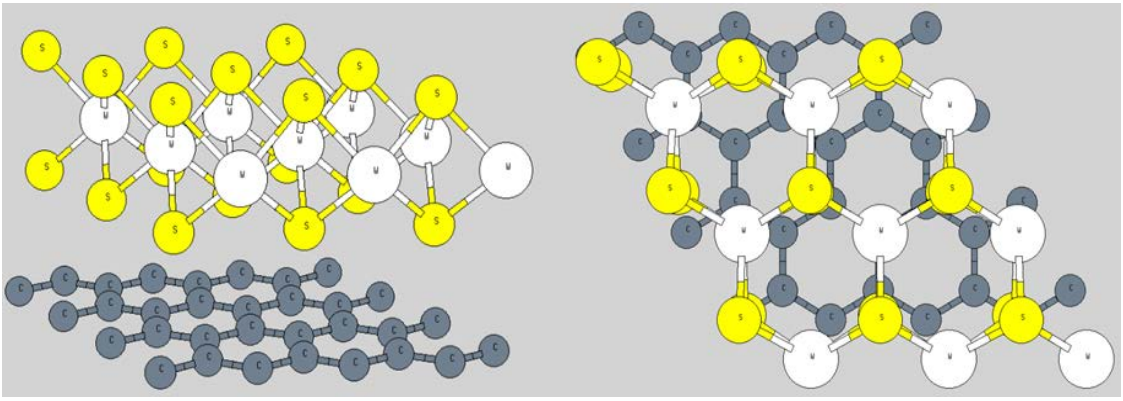

Figure 4.1: Side and top of view of the WS_2(3x3)/Graphene(4x4) heterostructure on TW configuration.

4.1.1 Structure of WS_2(3x3)/Graphene(4x4) supercell

As seen in Figure 4.2, the method we followed to constructed the heterostructure is to put the already discussed (in chapter 3) 3x3 SC of WS_2 monolayer over the 4x4 SC of graphene on TW configuration. The reason we chose TW configuration is because it exhibits the lowest total energy compared to others configurations. This heterostructure has hexagonal lattice structure and we performed DFT calculations in order to find the optimal structural parameters which minimize the total ground state energy of system. In this work, the geometry was defined by the following configuration for the lattice vectors $\mathbf{a_1}$, $\mathbf{a_2}$, $\mathbf{a_3}$:

$$\mathbf{a_1} = a\,(-1/2, \sqrt{3}/2, 0),\ \mathbf{a_2} = a\,(1, 0, 0),\ \mathbf{a_3} = c\,(0, 0, 1)$$

Figure 4.2

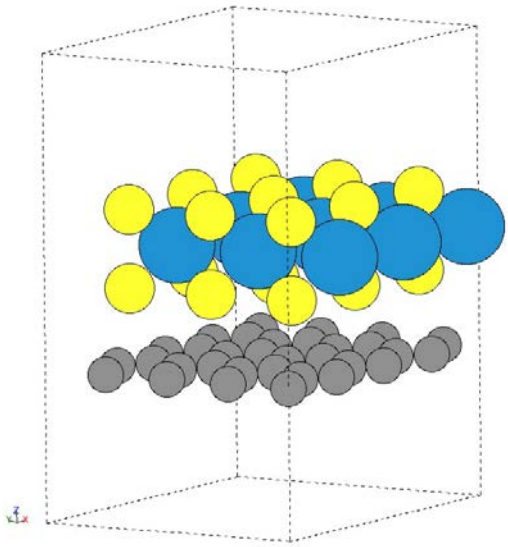

Figure 4.2: WS_2(3x3)/Graphene(4x4) supercell consist of 59 atoms 9W, 18S, 32C.

In order to define the optimal structural parameters for WS_2(3x3)/Graphene(4x4)

heterostructure we followed two calculations steps. In the first step we relaxed with stress tensor method the SC in TW configuration until the system converged to the minimum total energy and we obtained the structural parameters. We found lattice constant a=9.690Å and parameter u=0.621 (d_{s-s} = 3.096Å)[65] which determines the distance between sulfurs in the WS_2(3x3)/Graphene(4x4) heterostructure while keeping the parameter c=12Å fixed. Furthermore, we determined for the heterostructure the parameter z which describes the interlayer distance between the carbon atoms with the closest sulfur atoms plane according to the relation,

$$d_{c-s} = \left(u - \frac{1}{2} + z\right) * c - \frac{1}{4} * c \quad (32)$$

In this case we found the parameter z=0.408 that means interlayer distance of heterostructure d_{c-s}=3.348Å[63]. Afterwards, we got these initial structural parameters for WS_2(3x3)/Graphene(4x4) heterostructure and continued with DFT calculations for each parameter to confirm and improve the accuracy. Specifically, we performed some iterations with DFT for calculating the total energy of the system around lattice constant a=9.690Å while keeping the parameters u=0.621 (d_{s-s} = 3.096Å), z=0.408 (d_{c-s}=3.348Å) and c=12Å stable. The iterations started with lattice constant a of 9.65Å to 9.73Å with step 0.01Å and done for each value the calculation of total energy as we seen in Table.7.

Table.7

Energy (eV)	Lattice constant(Å)
-541.910	9.65
-541.937	9.66
-541.956	9.67
-541.968	9.68
-541.972	**9.69**
-541.970	9.70
-541.959	9.71
-541.941	9.72
-541.917	9.73

The energy curve E (eV) as a function of lattice constant a (Å) was fitted with a second degree polynomial of the form (31).

Figure 4.3

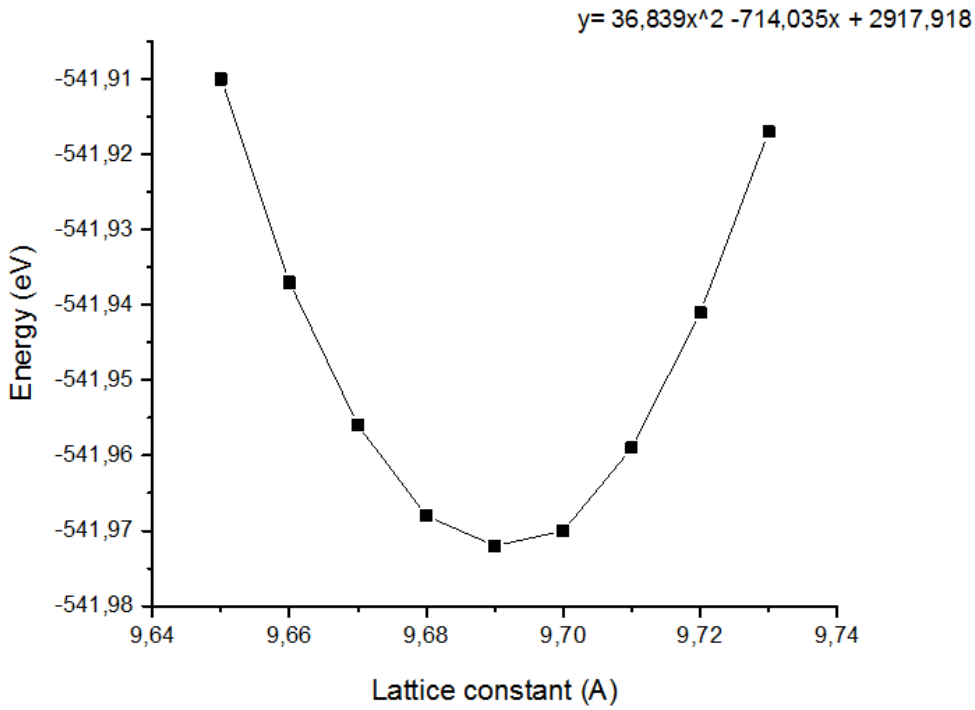

Figure 4.3 The energy curve E (eV) as a function of lattice constant a (Å) of WS_2(3x3)/Graphene(4x4) supercell.

Determining for minimum,

dy/dx = 2ax + b=0 => x= - b/(2a) =>x=9.690 we find **a=9.690Å, E_{min}=-541.972eV**

According to that result we determined the optimized lattice constant a=9.690Å for the WS_2(3x3)/Graphene(4x4) heterostructure. In order to make this equilibrium heterostructure we observed we have 2.60% the 3x3 SC of WS_2 monolayer stretched from the equilibrium state (a= 9.444Å) and also, we have compressed by 0.97% the 4x4 SC of graphene (a=9.785Å), respectively.

Afterwards, we followed the same procedure for the WS_2(3x3)/Graphene(4x4) heterostructure and we performed some iterations around of parameter u=0.621 (d_{s-s} = 3.096Å) while keeping lattice constant a=9.690Å, parameter z=0.408(d_{c-s}=3.348Å) and c=12Å stable.

The iterations began with u parameter of 0.618 to 0.625 with step 0.001 and done for each value the calculation of total energy as we seen in Table.8.

Table.8

Energy (eV)	Parameter u
-541.672	0.618
-541.820	0.619
-541.919	0.620
-541.972	**0.621**
-541.964	0.622
-541.905	0.623
-541.790	0.624
-541.618	0.625

The energy curve E (eV) (axis -y) as a function of parameter u (axis -x) was fitted with a second degree polynomial of the form (31).

Figure 4.4

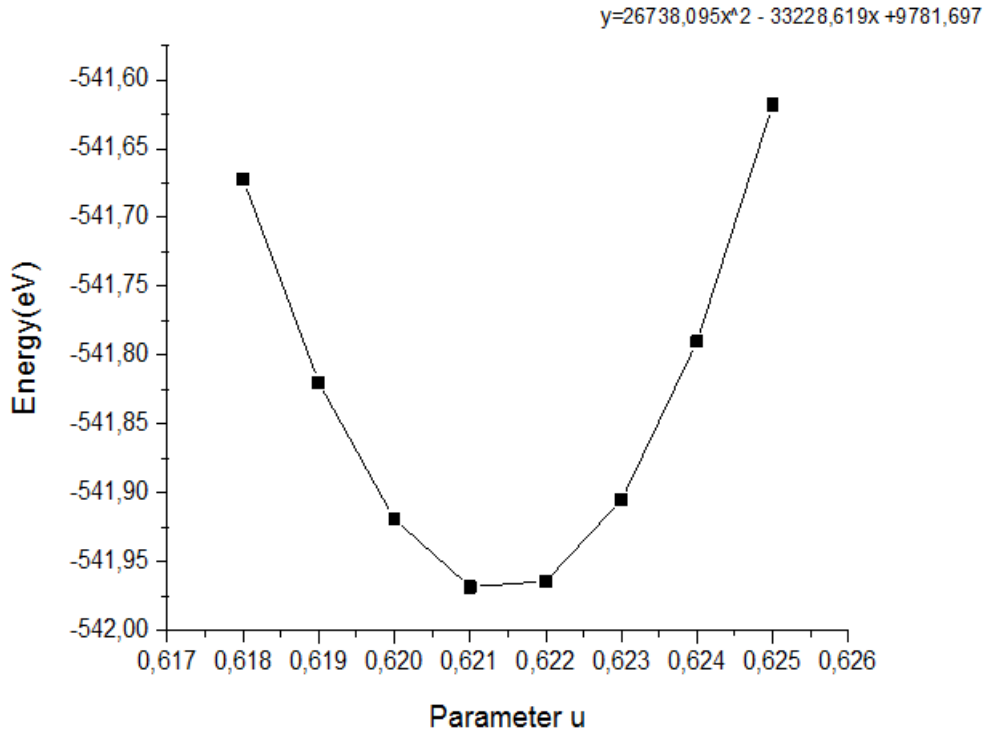

Figure 4.4 The energy curve E (eV) as a function of parameter u of WS_2(3x3)/Graphene(4x4) supercell.

Determining for minimum,

dy/dx = 2ax + b=0 => x= - b/(2a) =>x=0.621

we find **u=0.621 (d_{s-s}=3.096Å), E_{min}=-541.972eV**

According to these results, were determined the optimized super cell lattice parameters a=9.690Å, u=0.621 (d_{s-s}=3.096Å), c=12Å for the WS_2(3x3)/Graphene(4x4) heterostructure. We observe that in the heterostructure we have smaller distance d_{s-s}=3.096Å between sulfurs than in the 3x3 SC of WS_2 monolayer which is d_{s-s} = 3.144Å. That happened because the sulfur in WS_2 monolayer experienced van der Walls interactions with carbon atoms in graphene.

Finally, we repeated the same procedure to decide for the last parameter z which described the interlayer distance of heterostructure. We performed some iterations around of parameter z=0.408 (d_{c-s}=3.348Å) while keeping lattice constant a=9,690Å, parameter u=0.621 (d_{s-s}=3.096Å) and c=12Å stable. The iterations began with interlayer distance z of 0.405 to 0.410 with step 0.001 and each value the calculation of total energy is seen in Table.9.

Table.9

Energy (eV)	Distance z
-541.9711	0.405
-541.9723	0.406
-541.9728	**0.407**
-541.9726	0.408
-541.9723	0.409
-541.9714	0.410

The energy curve E (eV) as a function of parameter z was fitted with a second degree polynomial of the form (31).

Figure 4.5

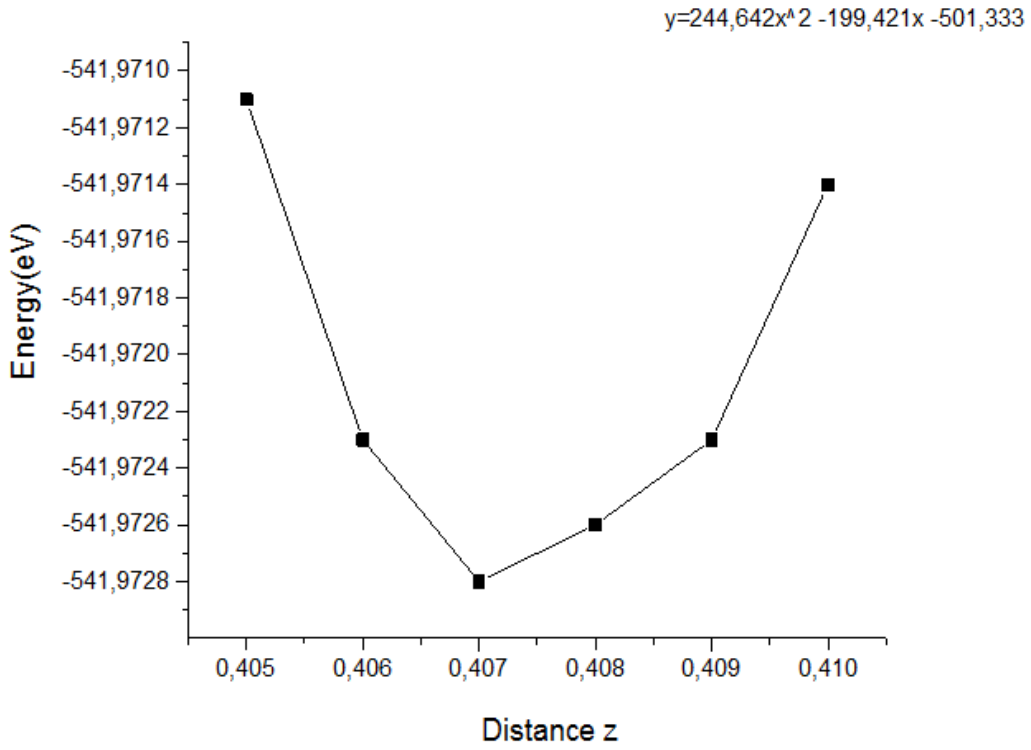

Figure 4.5: The energy curve E (eV) as a function of parameter z of WS_2(3x3)/Graphene(4x4) supercell.

Determining for minimum,

dy/dx = 2ax + b=0 => x= - b/(2a) =>x=0.407

we find **z=0.407 (d_{c-s}=3.336Å), E_{min}=-541.9728eV**

We found the optimized interlayer distance z=0.407 (d_{c-s}=3.336Å)[63][64][67] of WS_2(3x3)/Graphene(4x4) heterostructure. That value of interlayer distance of heterostructure agrees with other works. In conclusion, we have found all the optimized structural parameters of the heterostructure, and we calculate the binding energy based on the relation below:

$$E_{binding} = E_{WS2(3x3)/Graphene(4x4)} - E_{WS2(3x3)} - E_{Graphene(4x4)} \quad (33)$$

The binding energy of the WS_2(3x3)/Graphene(4x4) heterostructure was found to be 0.121eV. As we expected we have small binding energy because of weak interactions between layers. However, we have a positive value of the binding energy and this probably happened because we have a 2.60% lattice mismatch in the heterostructure.

4.1.2 Electronic band structure of WS_2(3x3)/Graphene(4x4) supercell

After studying the structure of WS_2(3x3)/Graphene(4x4) heterostructure and after we found the optimized structural parameters, we will discuss the electronic structure. We examine the results from DFT calculations for the electronic structure of the WS_2 (3 × 3)/Graphene (4 × 4) heterostructure to explain the behavior of the combined gapless semi-metallic graphene on the direct gap (1.945eV) WS_2 monolayer semiconductor. The Brillouin zone is a hexagon as we discussed in subsection 3.2.2 (Figure 3.15). We use the optimized supercell lattice parameters a=9.690Å, u=0.621 (d_{s-s}=3.096Å), z=0.407 (d_{c-s}=3.336Å), c=12Å and we perform DFT calculation for electronic band structure. In this electronic band structure calculation of heterostructure, we selected the M-K-G path in Brillouin zone to represent the results, as shown below (Figure 4.6).

Figure 4.6

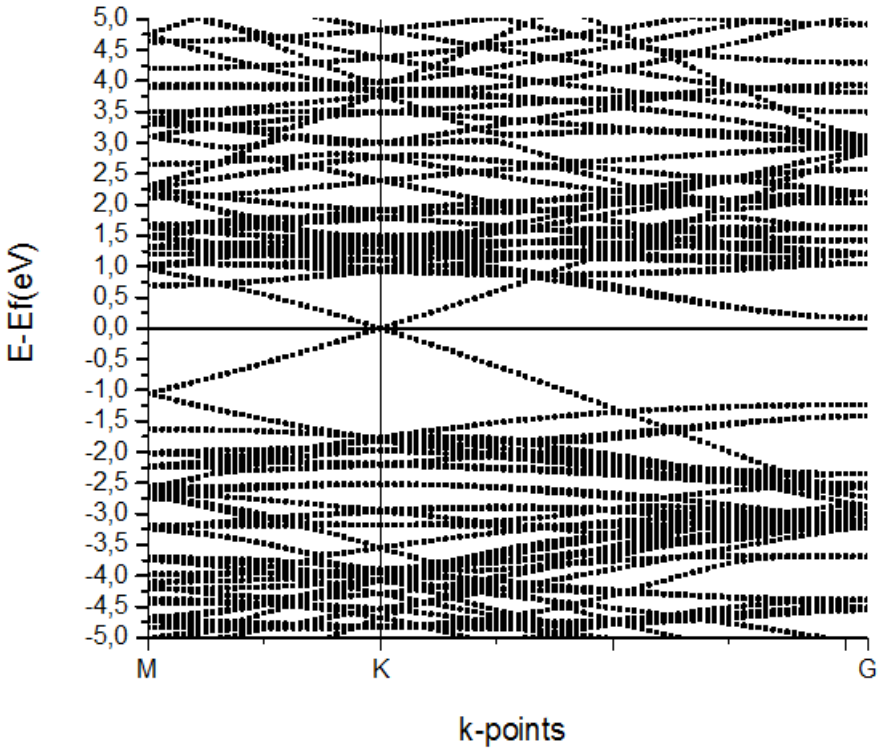

Figure 4.6: Bandstructure of WS_2(3x3)/Graphene(4x4) supercell.

As we see in the above band structure diagram we got zero band gap of the K-point and Fermi level was set to zero ($E-E_{fermi}$ = 0eV) with Fermi energy E_{fermi} = 0.556eV. We have the conduction band minimum (CBM) and the valence band maximum (VBM) meeting at a single point K for graphene, as expected. On the other hand, we expected for the WS_2 monolayer the conduction band minimum (CBM) and the valence band maximum (VBM) to coincide at the K point. However, we observed the CBM and the VBM for WS_2 monolayer shifted to the G-point[65][66]. The reason for this band alignment is due to 2.60% lattice mismatch of heterostructure and this results in a dislocation in the hexagonal Brillouin zone. In order to further investigate the band structure of the heterostructure and since we have many number of electronic

bands due to repeated periodicity of PC, we proceeded to the band structure unfolding of WS_2 (3 × 3)/Graphene (4 × 4) heterostructure.

This method as we described in section 2.2 aims to unfold the band structure of the SC to the PC. These band structure unfolding calculations help to fully understand the electronic structure as well as to explain the behavior of band alignment of the strained heterostructure. We start by calculating the electronic band structure unfolding of the WS_2(3x3)/Graphene(4x4) supercell with respect to the WS_2 monolayer PC. We selected the same M-K-G path in Brillouin zone to represented the result as shown below (Figure 4.7).

Figure 4.7

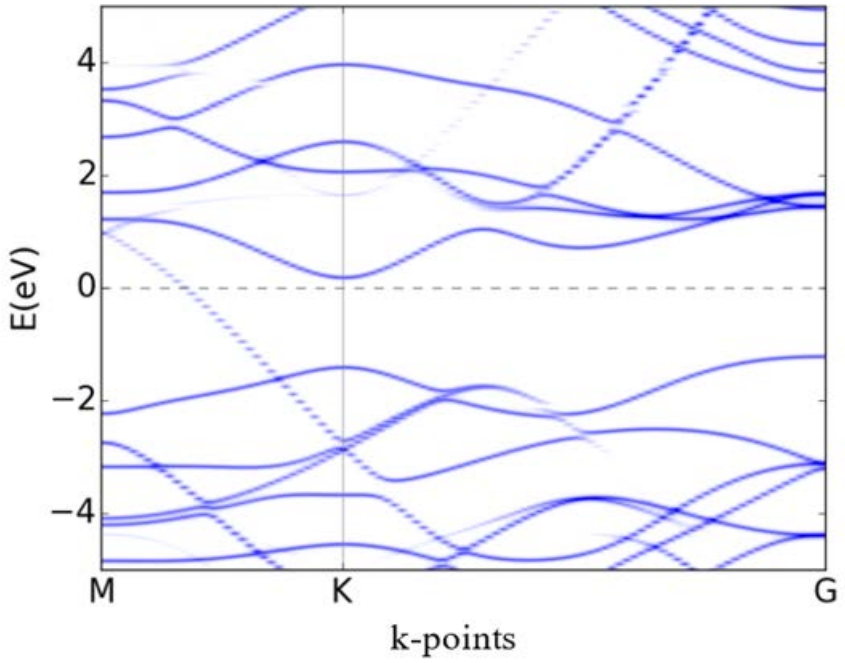

Figure 4.7: Bandstructure of the WS_2(3x3)/Graphene(4x4) supercell unfolded in the PC of WS_2 monolayer.

As we see in the above unfolded band structure diagram of the WS_2(3x3)/Graphene(4x4) supercell to the WS_2 monolayer PC, we observe a quite different electronic structure comparing to the unfolded band structure diagram of WS_2 supercell (subsection 3.1.4). In the case of the heterostructure we have an indirect band gap 1.672eV between VBM (G-point) and CBM (K-point) and we also observe a decreased gap (by 0.516eV) between VBM and CBM in M-point. That happened because of in order to made this equilibrium heterostructure we have 2.60% strained on 3x3 SC of WS_2 monolayer.

In order to complete the investigation of the electronic structure of the heterostructure we proceeded to another calculation for the unfolding electronic band structure of the WS_2(3x3)/Graphene(4x4) supercell to the graphene PC. We selected the same M-K-G path in Brillouin zone and the result is shown below.

Figure 4.8

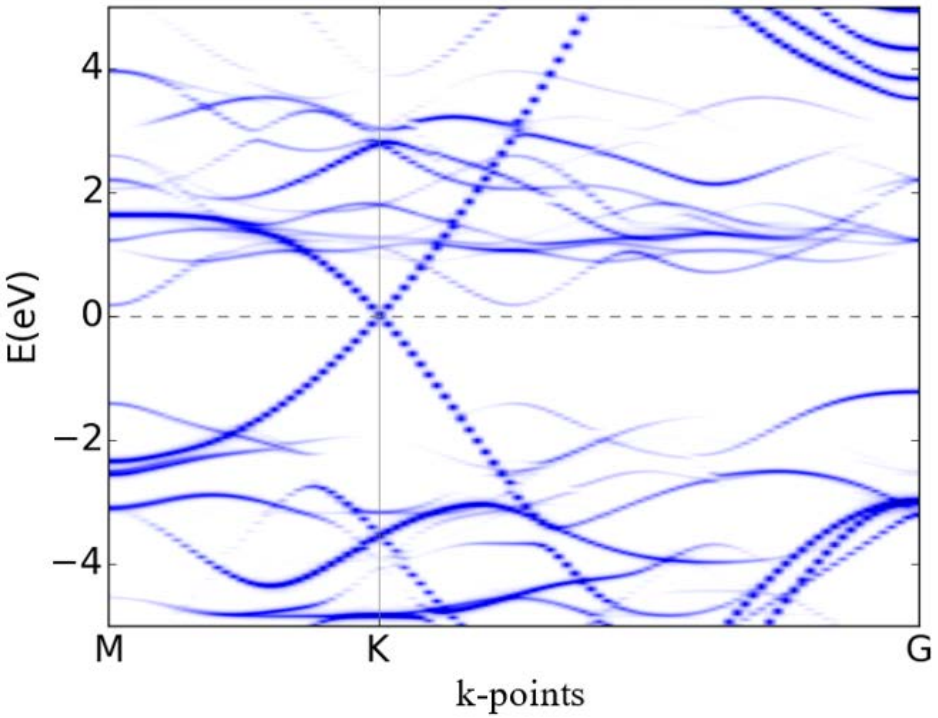

Figure 4.8: Bandstructure of the WS_2(3x3)/Graphene(4x4) supercell unfolded in the PC of graphene.

At this unfolded band structure diagram of the WS_2(3x3)/Graphene(4x4) supercell to the graphene PC, we observe the same characteristics compared to the unfolded band structure diagram of graphene supercell (subsection 3.2.4). In this equilibrium heterostructure the compression by 0.97% of the 4x4 SC of graphene does not influence the electronic structure. Based on these results we predict that the magnitude of lattice mismatch affects the electronic properties of the WS_2 monolayer of the heterostructure. In contrast, for lattice mismatch less than 1%, as is the case of graphene the electronic properties have not been influenced. In order to present more realistic electronic structure for the WS_2/Graphene heterostructure it is necessary to study a supercell with lattice mismatch less than 2.60%, as we do in the next section.

4.2 Heterostructure of WS_2(4x4)/Graphene(5x5)

In this section, we will move on to examine one more system of WS_2/Graphene heterostructure in order to achieve lattice mismatch less than 1%. We investigate the SC of the WS_2 (4 × 4)/Graphene (5 × 5) heterostructure which consists of 98 atoms as we see in Figure 4.9. We performed DFT calculations for the WS_2 (4 × 4)/Graphene (5 × 5) heterostructure to find the optimal structural parameters. We will discuss the theoretical results from DFT calculations for the electronic structure of the WS_2 (4 × 4)/Graphene (5 × 5) heterostructure and compare some results with the heterostructure of WS_2 (3 × 3)/Graphene (4 × 4) already studied.

Figure 4.9

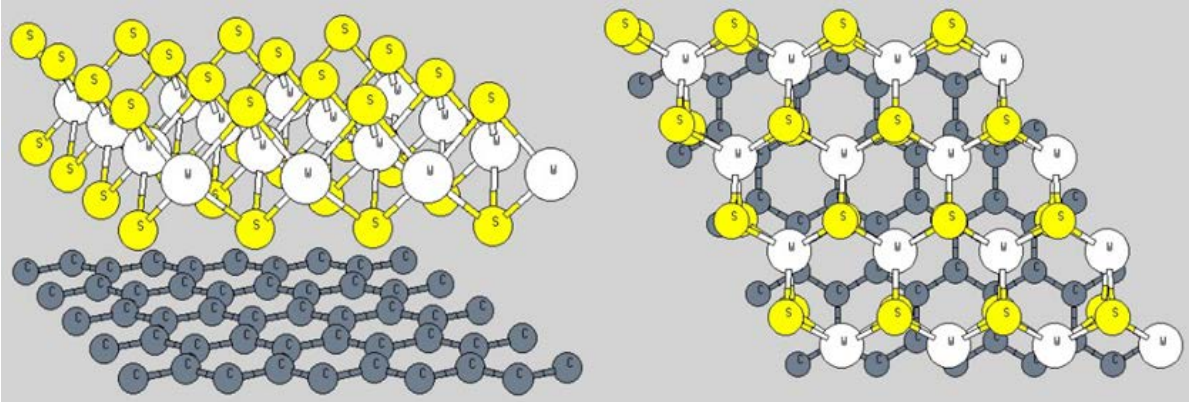

Figure 4.9: Side and top of view of the WS_2(4x4)/Graphene(5x5) heterostructure.

4.2.1 Structure of WS_2(4x4)/Graphene(5x5) supercell

In this subsection, we describe the structure of the WS_2 (4 × 4)/Graphene (5 × 5) heterostructure that we will study. We build a supercell of 4x4 unit cells of WS_2 monolayer on top of a supercell of 5x5 unit cells of graphene which consists of 98 atoms (16W, 32S, 50C) as we see in Figure 4.10. We investigated different configurations of the WS_2 (4 × 4)/Graphene (5 × 5) heterostructure like as TW (Top Tungsten) and TS (Top Sulfur) but the system exhibited the lowest total energy in another configuration after relaxed. This heterostructure has hexagonal lattice structure as expected and we performed DFT calculations in order to find the optimal structural parameters which minimize the total ground state energy of system.

The geometry is defined by the following configuration for the lattice vectors $\mathbf{a_1}$, $\mathbf{a_2}$, $\mathbf{a_3}$:

$$\mathbf{a_1} = a\,(-1/2, \sqrt{3}/2, 0),\ \mathbf{a_2} = a\,(1, 0, 0),\ \mathbf{a_3} = c\,(0, 0, 1)$$

Figure 4.10

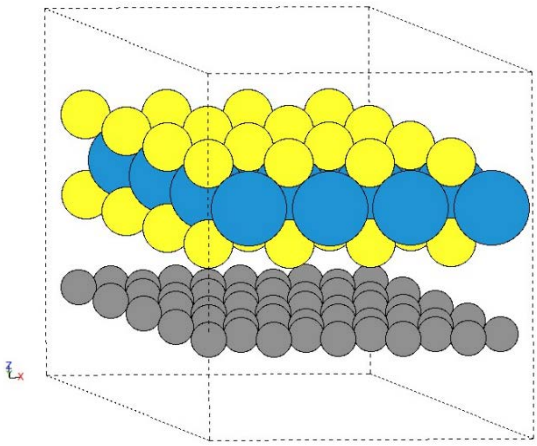

Figure 4.10: WS_2(4x4)/Graphene(5x5) supercell consist of 98 atoms 16W, 32S, 50C.

In order to define the optimal structural parameters of the WS_2(4x4)/Graphene(5x5) heterostructure we followed the same procedure as in subsection 4.1.1. We relaxed the SC of heterostructure until the system converged to the minimum total energy and then we measured the structural parameters.

We found lattice constant a=12.350Å and parameter u=0.617 which determines the distance between sulfurs ($d_{s\text{-}s}$=3.192Å)[65] in the WS_2(4x4)/Graphene(5x5) heterostructure while keeping the parameter c=12Å stable. Furthermore, we determined the parameter z which describes the interlayer distance between the carbon atoms with the closest sulfur atoms according to the relation (32) as we said in subsection 4.1.1. In this case we found the parameter z=0.414 which means that interlayer distance in the heterostructure is $d_{c\text{-}s}$=3.372Å[63][64][67]. Afterwards, we used these initially structural parameters for WS_2(4x4)/Graphene(5x5) heterostructure and continued with DFT calculations for each parameter to confirm and improve the accuracy. Specifically, we performed some iterations with DFT for calculating the total energy of the system around lattice constant a=12.350Å while keeping the parameters u=0.617 ($d_{s\text{-}s}$ = 3.192Å), z=0.414 ($d_{c\text{-}s}$=3.372Å) and c=12Å stable.

The iterations started with lattice constant a of 12.32Å up to 12.36Å with step 0.01Å and the results for the total energy as seen in Table.10.

Table.10

Energy (eV)	Lattice constant (Å)
-894.265	12.32
-894.284	12.33
-894.296	12.34
-894.300	**12.35**
-894.296	12.36

The energy curve E (eV) as a function of lattice constant a (Å) was fitted with a second degree polynomial of the form (31).

Figure 4.11

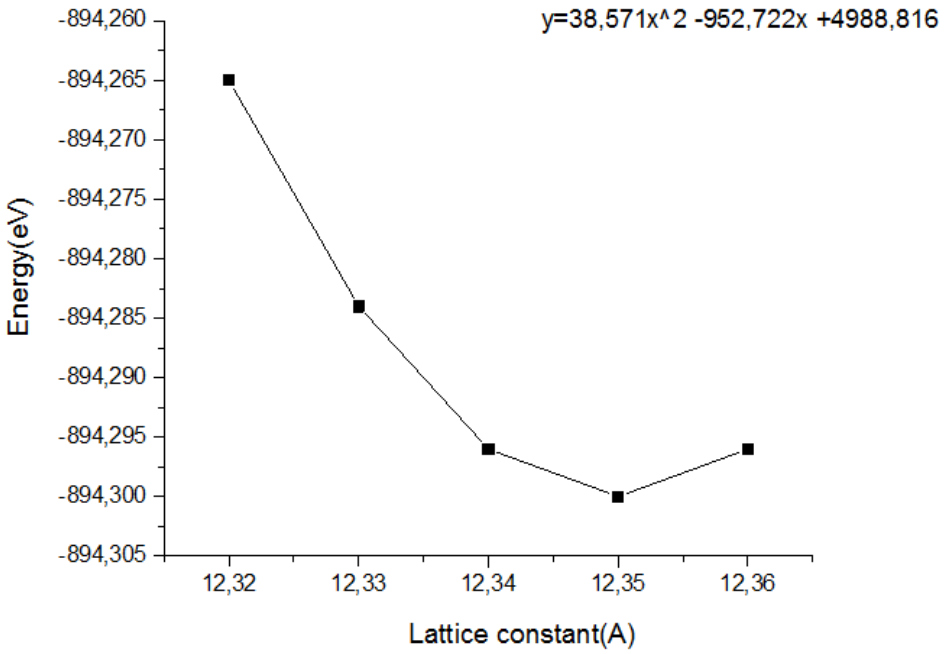

Figure 4.11: The energy curve E (eV) as a function of lattice constant a (Å) of WS_2(4x4)/Graphene(5x5) supercell.

Determining for minimum,

dy/dx = 2ax + b=0 => x= - b/(2a) =>x=12.350

we find **a=12.350Å, E_{min}=-894.300eV**

According to that result, we determined the optimized lattice constant a=12.350Å for the WS_2(4x4)/Graphene(5x5) heterostructure. We observe that we have 1.92% compressions of the 4x4 SC of WS_2 monolayer from the equilibrium state (a= 12.592Å) and also, we have stretched by 0.96% the 5x5 SC of graphene (a=12.232Å), respectively. That lattice mismatch of the heterostructure, will hopefully give a good description of the binding energy and electronic properties.

Afterwards, we followed the same procedure for the WS_2(4x4)/Graphene(5x5) heterostructure and we performed some iterations around u=0.617 (d_{s-s} = 3.192Å) while keeping lattice constant a=12.350Å, parameter z=0.414 (d_{c-s}=3.372Å) and c=12Å stable. The iterations began with u parameter of 0.614 to 0.620 with step 0.001 and done for each value the calculation of total energy as we seen in Table.11.

Table.11

Energy (eV)	Parameter u
-893.929	0.614
-894.146	0.615
-894.271	0.616
-894.300	**0.617**
-894.230	0.618
-894.059	0.619
-893.783	0.620

The energy curve E (eV) as a function of parameter u was fitted with a second degree polynomial of the form (31).

Figure 4.12

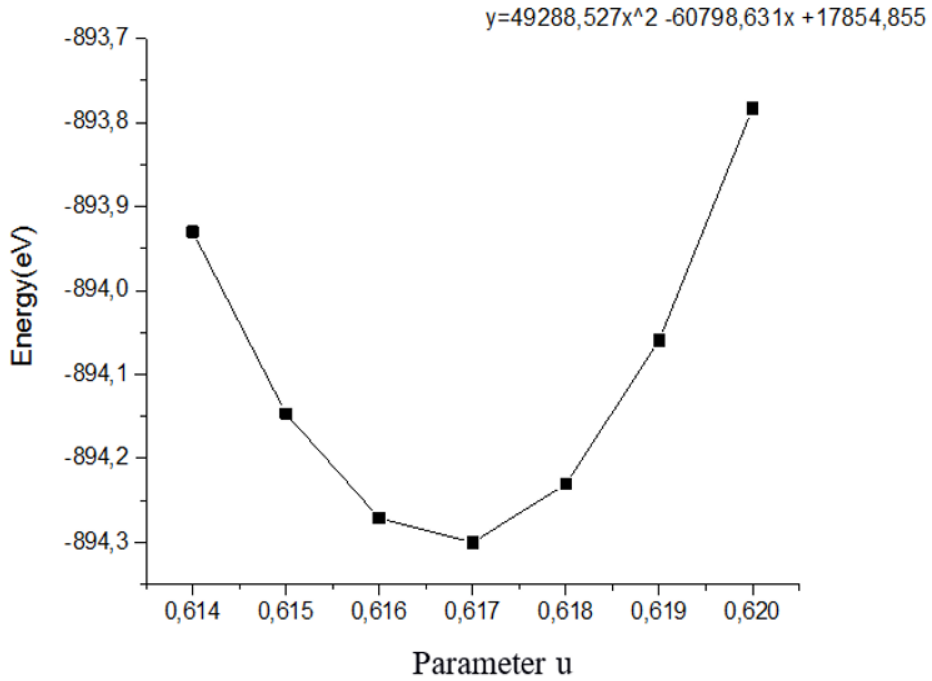

Figure 4.12: The energy curve E (eV) as a function of parameter u of WS_2(4x4)/Graphene(5x5) supercell.

Determining the minimum,

dy/dx = 2ax + b=0 => x= - b/(2a) =>x=0.617

we find **u=0.617 (d_{s-s} = 3.192Å), E_{min}=-894.300eV**

According to these results, the optimized super cell lattice parameters are a=12.350Å, u=0.617 (d_{s-s} = 3.192Å), c=12Å for the heterostructure. We observe that for the WS_2(4x4)/Graphene(5x5) heterostructure we have bigger distance u=0.617 (d_{s-s} = 3.192Å) between sulfurs atoms than WS_2(3x3)/Graphene(4x4) heterostructure, which has u=0.621 (d_{s-s}=3.096Å). The interlayer distance is bigger z=0.414 (d_{c-s}=3.372Å) than z=0.407 (d_{c-s}=3.336Å), respectively.

Finally, we repeated the same procedure to decide for last parameter z which described the interlayer distance of heterostructure. We performed some iterations around of parameter z=0.414 (d_{c-s}=3.372Å) while keeping lattice constant a=12.350Å, parameter u=0.617 (d_{s-s} = 3.192Å) and c=12Å stable.

The iterations began with interlayer distance z of 0.411 up to 0.416 with step 0.001 as seen in Table.12.

Table.12

Energy (eV)	Parameter z
-894.297	0.411
-894.299	0.412
-894.300	0.413
-894.300	**0.414**
-894.299	0.415
-894.297	0.416

The energy curve E (eV) as a function of parameter z was fitted with a second degree polynomial of the form (31).

Figure 4.13

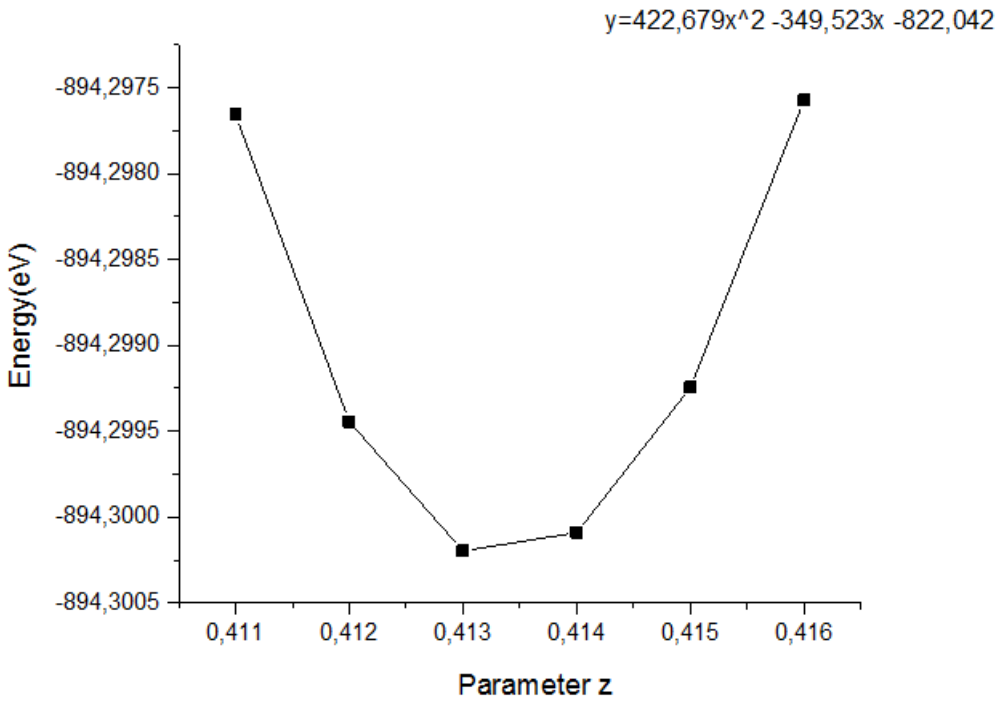

Figure 4.13: The energy curve E (eV) as a function of parameter z of WS_2(4x4)/Graphene(5x5) supercell.

Determining the minimum,

dy/dx = 2ax + b=0 => x= - b/(2a) =>x=0.414

we find **z=0.414 (d_{c-s}=3.372Å), E_{min}=-894.300eV**
We found the optimized interlayer distance z=0.414 (d_{c-s}=3.372Å) of WS_2(4x4)/Graphene(5x5) heterostructure and that is close to the interlayer distance d_{c-s}=3.336Å of the WS_2(3x3)/Graphene(4x4) heterostructure. Based on these agreements we determine that the WS_2(4x4)/Graphene(5x5) heterostructure are built successfully. In conclusion, according to these results we have found all the optimized structural parameters of the heterostructure. The binding energy of the WS_2(4x4)/Graphene(5x5) heterostructure was found to be -0.159eV. We have small binding energy because we have van der Waals interactions between the layers. The negative value of binding energy means that the heterostructure is stable.

4.2.2 Electronic band structure of WS_2(4x4)/Graphene(5x5) supercell

After determining the atomic structure of the WS_2(4x4)/Graphene(5x5) heterostructure and after we found the optimized structural parameters, we will discuss the electronic structure. We examined the theoretical results from DFT calculations in electronic structure for the WS_2(4x4)/Graphene(5x5) supercell to explain the behavior of combined gapless semi-metallic graphene on direct gap 1.945eV semiconductor WS_2 monolayer. The Brillouin zone is a hexagon as we discussed in subsection 3.2.2 (Figure 3.15). Based on the results of the structure of supercell WS_2(4x4)/Graphene(5x5) heterostructure we defined the optimized supercell lattice parameters a=12.350Å, u=0.617 (d_{s-s}=3.192Å), z=0.414 (d_{c-s}=3.372Å), c=12Å and we performed DFT calculation for electronic band structure. In this electronic band structure calculation of heterostructure, we selected the M-K-G path in Brillouin zone to represented the result as shown below (Figure 4.14).

Figure 4.14

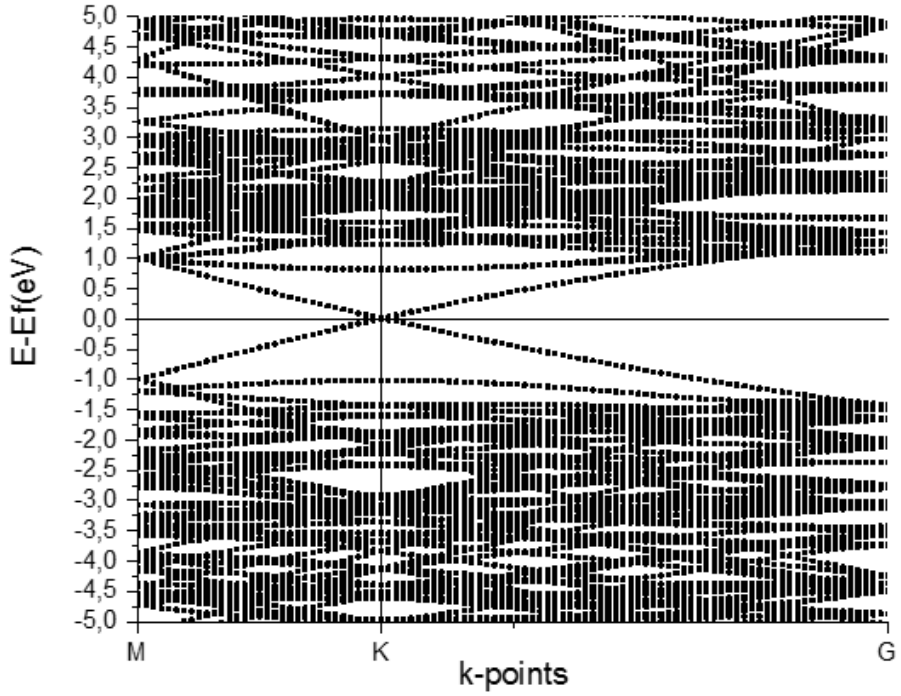

Figure 4.14: Bandstructure of WS_2(4x4)/Graphene(5x5) supercell.

As we see in the above band structure diagram we measured zero band gap at the K-point and Fermi level was set to zero ($E-E_{fermi} = 0eV$) with Fermi energy E_{fermi} = 0.581eV of heterostructure. We have the conduction band minimum (CBM) and the valence band maximum (VBM) meeting at a single point K that describes the behavior of graphene in the heterostructure, as expected. Additionally, we observe for the WS_2 monolayer the conduction band minimum (CBM) and the valence band maximum (VBM) band alignment with graphene at the K point[63]. This electronic structure of the WS_2(4x4)/Graphene(5x5) heterostructure is quite different from the WS_2(3x3)/Graphene(4x4) heterostructure. The explanation comes from the 1.92% lattice mismatch of the WS_2(4x4)/Graphene(5x5) heterostructure resulting in we have smaller dislocation in the hexagonal Brillouin zone and this allows us to reproduced more efficient and reliable the electronic structure for WS_2/Graphene heterostructures.

In order to a deeper understanding of the band structure of heterostructure because we have many number of electronic bands due to repeated periodicity of PC, we proceeded to the band structure unfolding method of the WS_2 (4 × 4)/Graphene (5 × 5) heterostructure. This method as we described in section 2.2 aim to unfolding the band structure of the SC to the PC. This band structure unfolding calculation we helped to clearly understanding how influence the electronic structure of each monolayer on heterostructure if we have lattice mismatch less than 1%. We calculated electronic band structure unfolding of the WS_2(4x4)/Graphene(5x5) supercell to the WS_2 monolayer PC. We selected the same M-K-G path in Brillouin zone to represented the result as shown below.

Figure 4.15

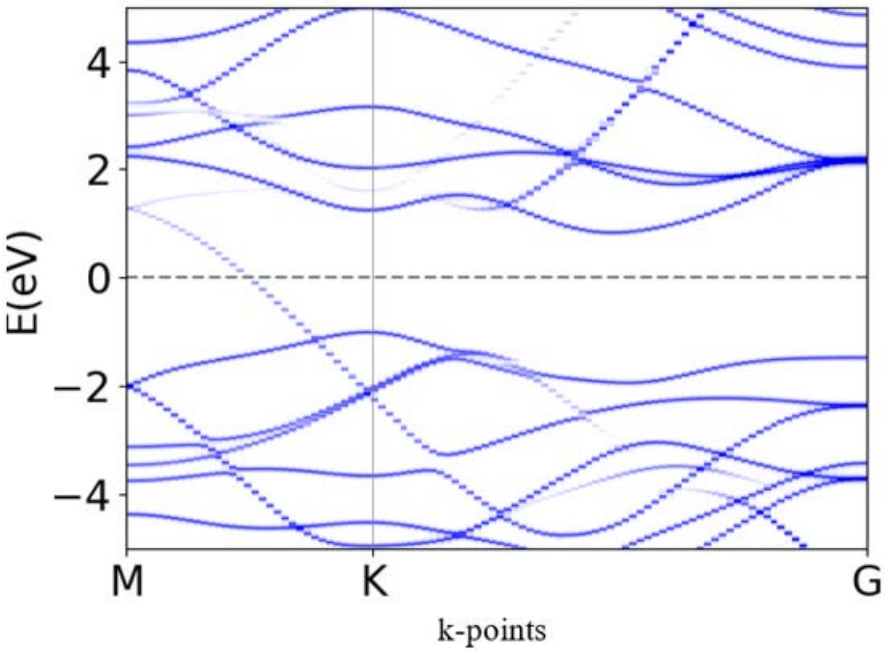

Figure 4.15: Bandstructure of the WS_2(4x4)/Graphene(5x5) supercell unfolded in the PC of WS_2 monolayer.

As we see in the above unfolding band structure diagram of the WS_2(4x4)/Graphene(5x5) supercell to the WS_2 monolayer PC we observed small differences of the electronic structure compared to the unfolding band structure diagram of WS_2 supercell (subsection 3.1.4). In this case of heterostructure we have an indirect band gap 1.992eV between VBM near to K-point and CBM where it is between K-point and G-point. We also, observed opened a gap by 0.295eV between VBM and CBM in M-point. The small differences on unfolding band structure diagram we happened because of in order to made this equilibrium WS_2(4x4)/Graphene(5x5) heterostructure we have 1.92% compressed on 4x4 SC of WS_2 monolayer. These results confirm that the magnitude of tensile strain or compression is very sensitive quantity and affects to the pure electronic properties of WS_2 monolayer on heterostructure even though we have lattice mismatch less than 1%.

Chapter 5

Excitons in monolayer WS_2

In this chapter, we use the approximation methods RPA, BSE and BSE-truncated as we described in section 2.3, in order to find the macroscopic dielectric function $\varepsilon_M(\omega)$ as well as to extract the optical ABS from imaginary its part. We absorption calculated the longitudinal part of 2D polarizability to we determine the excitation effects for monolayer of WS_2. Based on these, we investigated firstly the excitation effects in the optimal equilibrium structure of WS_2 monolayer (determined in subsection 3.1.1) and then we performed these calculations with isotropically stretching and compressing the WS_2 monolayer. The reason we did these calculations is to see how strain on a monolayer WS_2 affects the optical ABS. We performed DFT calculations and used the approximations methods RPA, BSE and BSE-truncated to calculate the longitudinal part of 2D polarizability to investigate excitons of monolayer WS_2, the results are shown in Figure 5.1. We used the optimal equilibrium structure of monolayer WS_2 with unit cell lattice parameters a=3.148Å, u=0.619 ($d_{s\text{-}s}$=3.144Å), c=12Å, as determined in subsection 3.1.1. In our calculation, we use the computational details as we discussed in section 2.4 but for k-points sampling we replaced with large density of k-points (k_x, k_y, k_z) = (30, 30, 1)[71] which are required for the BSE spectrum of 2D systems to converge. The noninteracting response function χ^0 was constructed

from LDA wave functions and the PW cutoff for the response function (local-field effects) was set to 50eV.

Figure 5.1

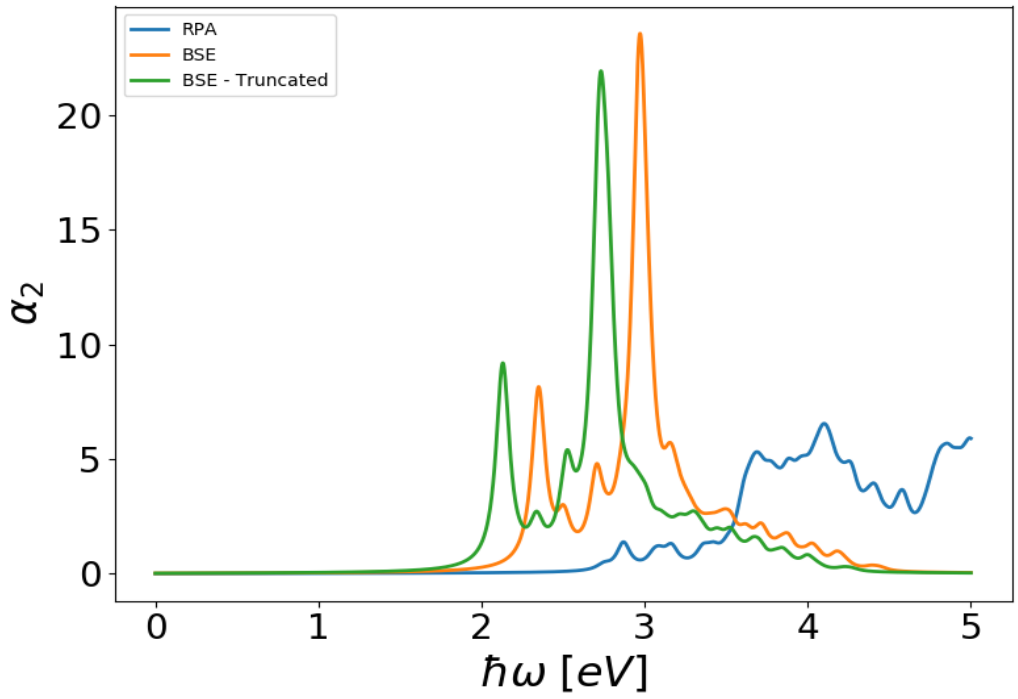

Figure 5.1: Polarizability of monolayer WS_2 calculated with the RPA, BSE and BSE truncated.

The resulting spectrum for monolayer WS_2 is shown above in Figure 5.1. We observed that for BSE polarizability with Coulomb truncation we obtain the A exciton in 2.130eV but for BSE polarizability without Coulomb truncation we measure 2.350eV, whereas RPA does not show an exciton peak (due to the RPA calculation neglecting electron hole interactions). The excitonic effects are much stronger due to the reduced screening in 2D. In particular, we can identify a distinct exciton well below the band edge. We saw that without Coulomb truncation, the BSE spectrum is shifted upward in energy due the screening of electron-hole interactions from periodic images. Experimentally, the absorption spectrum of monolayer WS_2 exhibits for A exciton peak around 2.02eV[72]. According to these, the theoretical results from BSE spectrum, (and specifically for Coulomb truncated) we represent show a reliable approximation method to describe and predict the excitation effects for 2D materials, with good agreement of experimental results. After we investigated the excitation effects for equilibrium structure of monolayer WS_2, we move on to studied the excitons in strained monolayer WS_2. We applied isotropic stretching by 5% and 10% in the equilibrium structure of monolayer WS_2. We performed for each case DFT calculations and used the approximations methods RPA, BSE and BSE-truncated to calculate the longitudinal part of 2D polarizability. In the case of 5% stretched monolayer WS_2, the lattice constant is a=3.198Å and for 10% stretched a=3.248Å. The other unit cell lattice parameters as well as computational details for RPA and BSE methods are the

same as in the equilibrium structure. The resulting spectra for 5% and 10% stretched monolayer WS_2 are shown below in Figure 5.2 and Figure 5.3, respectively.

Figure 5.2

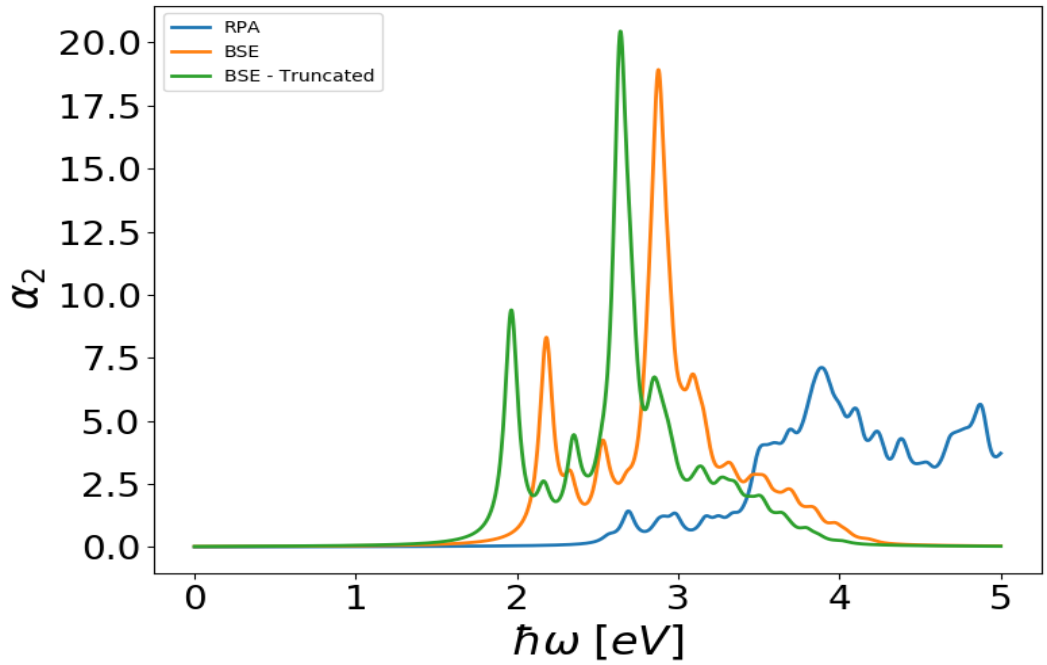

Figure 5.2: Polarizability of 5% stretched monolayer WS_2 calculated with the RPA, BSE and BSE truncated.

Figure 5.3

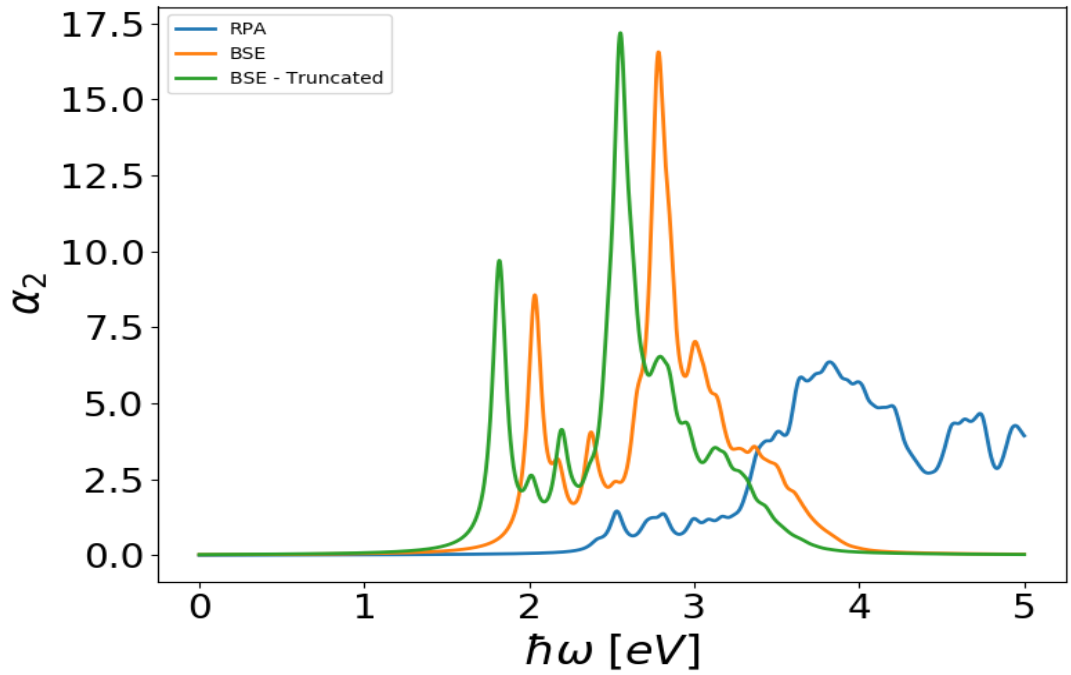

Figure 5.3: Polarizability of 10% stretched monolayer WS_2 calculated with the RPA, BSE and BSE truncated.

For the cases of the stretched monolayer WS_2, the results for the A exciton for each approximations method are shown below in Table.13.

Table.13

Monolayer of WS_2	Stretched 5%	Stretched 10%
Exciton	A	A
RPA	-	-
BSE	2.182eV	2.034eV
BSE truncated	1.965eV	1.818eV

We observe that for stretched by 5% and 10% monolayer WS_2, the energies of excitons decreased compared to the equilibrium structure. In the case of stretched by 5% in monolayer WS_2 (Figure 5.2) we saw that the BSE spectrum with Coulomb truncation, is shifted downward 0.165eV for A exciton compare to the ABS of monolayer WS_2 at equilibrium (Figure 5.1). On the other hand, in the case of stretched by 10% in monolayer WS_2 (Figure 5.3), we see that the spectrum for BSE-truncated is shifted even further downward by 0.312eV for A exciton. Furthermore, again in both cases without Coulomb truncation, the BSE spectrum is shifted upward in energy due the screening of electron hole interactions from periodic images, whereas RPA does not show any exciton peak. These results are clues that the stretching of monolayer WS_2 affect directly in the optical ABS. A reasonable explanation for that is quantum confinement[73] as discussed later. In this case, the size of the unit cell increases in monolayer WS_2, this means increased to confining dimension makes the motion of randomly moving electron less restricted.

We examined the excitation effects for the case of stretched monolayer WS_2, we move on to study the excitons in the case of compressed monolayer WS_2. We applied isotropic compressive strain by 5% and 10% in the equilibrium structure of monolayer WS_2. We performed for each case DFT calculations and used the approximations methods RPA, BSE and BSE truncated to calculate the longitudinal part of 2D polarizability. In the case of 5% compressed monolayer WS_2, the lattice constant is a=3.098Å and for 10% compressed was set in a=3.048Å. The other unit cell lattice parameters as well as computational details for RPA and BSE methods are the same as in the equilibrium structure. The resulting spectra for 5% and 10% compressed monolayer WS_2 are shown below in Figure 5.4 and Figure 5.5 respectively.

Figure 5.4

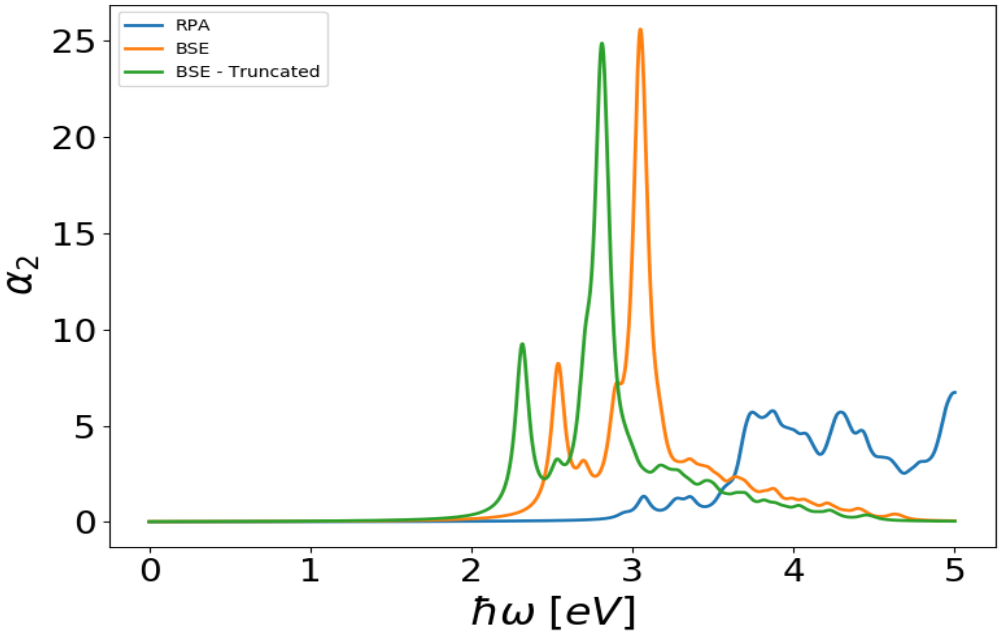

Figure 5.4: Polarizability of 5% compressed monolayer WS_2 calculated with the RPA, BSE and BSE truncated.

Figure 5.5

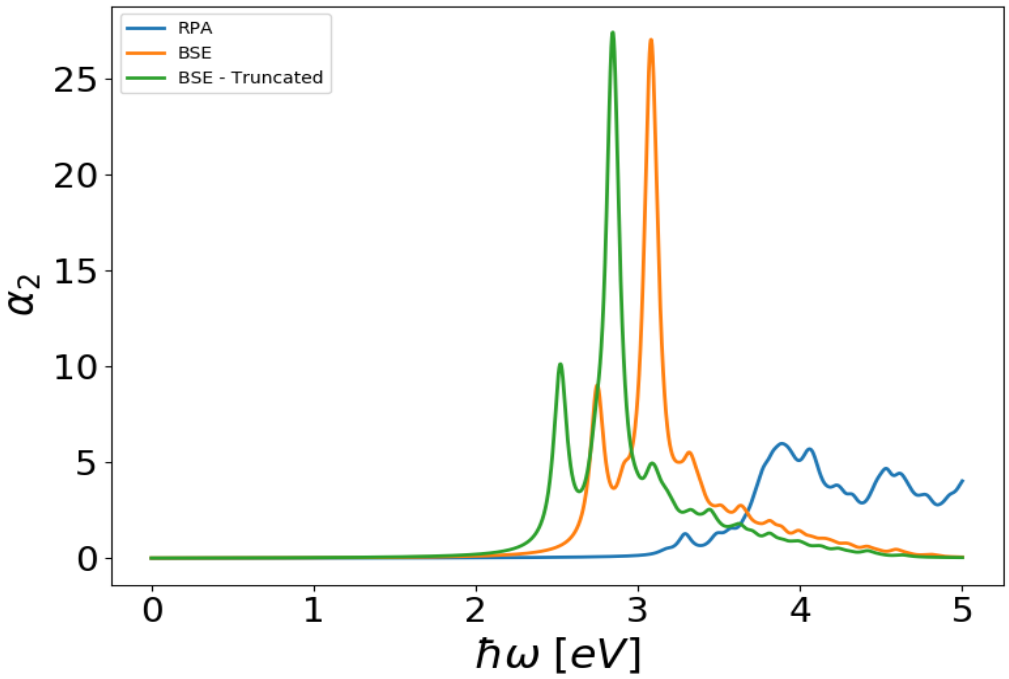

Figure 5.5: Polarizability of 10% compressed monolayer WS_2 calculated with the RPA, BSE and BSE truncated.

For these cases of compressed monolayer WS_2 the results for the A exciton for each approximation method are shown below in Table.14.

Table.14

Monolayer of WS_2	Compressed 5%	Compressed 10%
Exciton	A	A
RPA	-	-
BSE	2.539eV	2.749eV
BSE truncated	2.316eV	2.522eV

According to these results, we observe that for 5% and 10% compression of monolayer WS_2 the energies of excitons increase compared to the equilibrium structure of monolayer WS_2. In the case of 5% compression (Figure 5.4), we see that the BSE spectrum with Coulomb truncation, is shifted upward 0.186eV for A exciton compared to the equilibrium monolayer WS_2 (Figure 5.1). On the other hand, in the case of 10% compression of monolayer WS_2 (Figure 5.5), we see that the spectrum for BSE-truncated is shifted even further upward with 0.392eV for A exciton compared to the equilibrium monolayer WS_2. Furthermore, we see again in both cases that without Coulomb truncation, the BSE spectrum is shifted upward in energy due the screening of electron hole interactions from periodic images, whereas RPA does not show any exciton peaks. These results show that compression of monolayer WS_2 influence the spectrum. The explanation is the same such as in case of the stretched monolayer WS_2 and is due to the quantum confinement effect.

In conclusion, in this chapter we saw that the BSE spectrum with Coulomb truncation for monolayer WS_2 produced the best results to describe and predict the excitation effects in agreement with experimental results. We observed also, that the strained

(stretch or compress) monolayer WS_2 influence significantly the photoluminescence as well as the excitation effects due to quantum confinement effect.

Chapter 6

Conclusions

In this work, we performed first principles calculations in order to investigate the electronic properties of WS_2/Graphene bilayers. We used GPAW, an open source python code based on projector-augmented wave (PAW) method and the atomic simulation environment (ASE). In the DFT calculations for the atomic and electronic structure we chose LDA for the exchange-correlation functional and the parameter "setups = {'W': '6'}", that is six valence electrons for W atom, which proved vital to provide the best description for the structural and electronic properties of monolayer WS_2, graphene, and WS_2/graphene heterostructure.

More specifically, we achieved percentage error less than 0.6% for the atomic structure parameters, such as lattice constants, comparing with experimental values for both graphene and WS_2 monolayer. With our electronic band structure calculations, we confirmed the semiconducting (direct band gap) characteristics for the monolayer WS_2 and for graphene we observed the Dirac cone in the Brillouin zone which describes the semi-metallic (band gap free) behavior, as expected. Furthermore, we used the electronic band structure unfolding method for supercell calculations, which proved an extraordinary and reliable process to reproduce the true electronic band structure of monolayer WS_2 and graphene supercells.

Our theoretical investigation of different WS_2/Graphene heterostructures showed that lattice mismatch plays a crucial role in these hetero-bilayers. For the WS_2(3x3)/Graphene(4x4) supercell in its equilibrium configuration, we found that the WS_2 monolayer was stretched by 2.60%, with important consequences for the stability of the heterostructure and its electronic band structure. We observed an indirect band gap transition (G-K) with a value of 1.672 eV compared to the direct (K-K) 1.945eV band gap in equilibrium monolayer WS_2. However, the compression by 0.97% of graphene in the equilibrium heterostructure does not have any visible influence on the electronic band structure. On the other hand, we found that in the equilibrium WS_2(4x4)/Graphene(5x5) supercell there is a 1.92% compression of monolayer WS_2. Although we obtained a stable heterostructure in this case, the electronic band structure was affected showing an indirect transition with a 1.992eV band gap between the valence band maximum near the K-point and the conduction band minimum shifted near to the Γ-point. We also observed a gap widening by 0.295eV between valence band maximum and conduction band minimum at the M-point comparing to the electronic band structure of the equilibrium free-standing monolayer. Graphene was stretched by 0.96% in the equilibrium heterostructure but this had not influence on the electronic structure of the WS_2(4x4)/Graphene(5x5) heterostructure. Based on these results, it is clear that the indirect transitions as well as the miss-crossing band alignment in the electronic band structure of WS_2/Graphene heterostructures is due to the strained supercells of monolayer WS_2. Our results are in agreement with previous theoretical studies on strained monolayer TMDs and indicate that the graphene substrate may modify monolayer WS_2 band structure through strain. Moreover, the small strain on the graphene layer has no effect in its semi-metallic properties inside WS_2/Graphene heterostructures.

In this work, we also studied excitonic effects in monolayer WS_2 by following different approximation methods such as RPA, BSE and BSE-truncated. We obtained the best description from the BSE spectrum with Coulomb truncation due to the reduced

screening in 2D. We find a peak at 2.130eV for the exciton and at 2.732eV for the band gap. We observed that for strained monolayer WS_2, by 5% and 10%, the absorption spectrum changes significantly in a way which is totally consistent with quantum confinement effects.

Theoretical investigation of 2D materials, such as monolayer WS_2 and graphene as well as WS_2/Graphene heterostructures in our case, gives fascinating results for the atomic and electronic structure which may lead to the controlled manipulation of electrical and optical properties in these 2D materials. These materials, single layers as well as vdW heterostructures, are great candidates for technological applications.

References

[1] D. Xiao, G.-B. Liu, W. Feng, X. Xu, and W. Yao, “Coupled spin and valley physics in monolayers of mos2 and other group-vi dichalcogenides,” Phys. Rev. Lett, vol. 108, p. 196802, 2012.

[2] A. K. Geim & K. S. Novoselov, “The rise of graphene”, Nature Materials 6, pages 183 – 191, 2007.

[3] Daphne Davelou, Georgios Kopidakis, George Kioseoglou, and Ioannis N. Remediakis, “MoS2 nanostructures: Semiconductors with metallic edges”, Solid State Communications, 192:42{46, 2014.

[4] Hannu Pekka Komsa and Arkady V. Krasheninnikov, “Two-dimensional transition metal dichalcogenide alloys: Stability and electronic properties”, Journal of Physical Chemistry Letters, 3(23):3652{3656, 2012.

[5] K. S. Novoselov, D. Jiang, F. Schedin, T. J. Booth, V. V. Khotkevich, S. V. Morozov, and A. K. Geim, ”Two-dimensional atomic crystals”, Proceedings of the National Academy of Sciences of the United States of America 102, 10451, 2005.

[6] Vasilios Georgakilas, Michal Otyepka, Athanasios B. Bourlinos, Vimlesh Chandra, Namdong Kim, K. Christian Kemp, Pavel Hobza, Radek Zboril and Kwang S. Kim, “Functionalization of Graphene: Covalent and Non-Covalent Approaches, Derivatives and Applications”, Chem. Rev, 112 (11), pp 6156–6214, 2012.

[7] Lin YM, Dimitrakopoulos C, Jenkins KA, Farmer DB, Chiu HY, Grill A, Avouris P, “100-GHz transistors from wafer-scale epitaxial graphene”, Science, 327, 662, 2010.

[8] Liu M, Yin X, Ulin-Avila E, Geng B, Zentgraf T, Ju L, Wang F, Zhang X, “A graphene-based broadband optical modulator”, Nature, 474, 64, 2011.

[9] Kim KS, Zhao Y, Jang H, Lee SY, Kim JM, Kim KS, Ahn JH, Kim P, Choi JY, Hong BH,” Large-scale pattern growth of graphene films for stretchable transparent electrodes”, Nature, 457, 706, 2009.

[10] Zhu Y, Murali S, Stoller MD, Ganesh KJ, Cai W, Ferreira PJ, Pirkle A, Wallace RM, Cychosz KA, Thommes M, Su D, Stach EA, Ruoff RS,” Carbon-based supercapacitors produced by activation of graphene”, Science, 332, 1537, 2011.

[11] El-Kady MF, Strong V, Dubin S, Kaner RB,” Laser scribing of high-performance and flexible graphene-based electrochemical capacitors”, Science, 335, 6074, 2012.

[12] Xi Yang, Mingsheng Xu, Weiming Qiu, Xiaoqiang Chen,[a] Meng Deng, Jinglin Zhang, Hideo Iwai, Eiichiro Watanabe and Hongzheng Chen, “Graphene uniformly decorated with gold nanodots: *in situ* synthesis, enhanced dispersibility and applications”, Mater. Chem, 21, 8096, 2011.

[13] Deng, M, Yang, X, Silke, M. Qiu, W. M. Xu, M. S. Borghs, G. Chen, H. Z. “Sensors Actuators B”, Chem, 158, 176, 2011.

[14] Mingsheng Xu, Daisuke Fujita, Nobutaka Hanagata," Perspectives and Challenges of Emerging Single-Molecule DNA Sequencing Technologies", small, 5, No. 23, 2638–2649, 2009.

[15] S. Garaj, W. Hubbard, A. Reina, J. Kong, D. Branton & J. A. Golovchenko," Graphene as a subnanometre trans-electrode membrane", Nature, 467, 190, 2010.

[16] MingSheng Xu, Yan Gao, Xi Yang, HongZheng Chen," Unique synthesis of graphene-based materials for clean energy and biological sensing applications", Chin. Sci. Bull, 57, 3000, 2012.

[17] Q. H. Wang, K. Kalantar-Zadeh, A. Kis, J. N. Coleman, M. S. Strano, "Electronics and optoelectronics of two-dimensional transition metal dichalcogenides", Nat.Nanotechnol, 7, 699, 2012.

[18] J.A.Wilson, A.D.Yoffe, "The transition metal dichalcogenides discussion and interpretation of the observed optical, electrical and structural properties", Adv.Phys, Volume 18, 1969, Pages 193-335, 2006.

[19] Francesco Bonaccorso, Tawfique Hasan, Zhipei Sun, Luigi Colombo, Andrea C.Ferrari, "Production and processing of graphene and 2d crystals", Mater. Today, Volume 15, Issue 12, Pages 564-589, 2012.

[20] Gwan-Hyoung Lee, Young-Jun Yu, Xu Cui, Nicholas Petrone, Chul-Ho Lee, Min Sup Choi, Dae-Yeong Lee, Changgu Lee, Won Jong Yoo, Kenji Watanabe, Takashi Taniguchi, Colin Nuckolls, Philip Kim, and James Hone, "Flexible and Transparent MoS_2 Field-Effect Transistors on Hexagonal Boron Nitride-Graphene Heterostructures", ACS Nano, 7 (9), pp 7931–7936, 2013.

[21] Kin Fai Mak, Changgu Lee, James Hone, Jie Shan, and Tony F. Heinz, "Atomically Thin MoS_2: A New Direct-Gap Semiconductor", Physical Review Letters, 105(13):136805, 2010.

[22] Damien Voiry, Hisato Yamaguchi, Junwen Li, Rafael Silva, Diego C B Alves, Takeshi Fujita, Mingwei Chen, Tewodros Asefa, Vivek B Shenoy, Goki Eda, and Manish Chhowalla, "Enhanced catalytic activity in strained chemically exfoliated WS_2 nanosheets for hydrogen evolution", Nature materials, 12(9):850-5, 2013.

[23] P. Hohenberg and W. Kohn, "Inhomogeneous Electron Gas", Phys. Rev. 136, B864, 1964.

[24] W. Kohn and L. J. Sham, "Self-Consistent Equations Including Exchange and Correlation Effects", Physical Review B, 140(1951), 1965.

[25] D. Bohm and D. Pines, "A Collective Description of Electron Interactions. I. Magnetic Interactions", Phys. Rev, 82, 625–634, 1951.

[26] Hendrik J. Monkhorst and James D. Pack, "Special points for Brillouin-zone integrations", Phys. Rev, B 13, 5188–5192, 1976.

[27] T. G. Dargam, R. B. Capaz, and Belita Koiller, “Disorder and size effects in the envelope-function approximation”, Phys. Rev. B 56, 9625, 1997.

[28] L.W. Wang, L. Bellaiche, S.-H. Wei, and A. Zunger, “Majority Representation of Alloy Electronic States”, Phys. Rev. Lett. 80, 4725, 1998.

[29] V. Popescu and A. Zunger, ”Extracting E versus $\vec{k}$ effective band structure from supercell calculations on alloys and impurities”, Phys. Rev, B 85, 085201, 2012.

[30] D. Pines and D. Bohm, ”A Collective Description of Electron Interactions: II. Collective vs Individual Particle Aspects of the Interactions”, Phys. Rev. 85, 338–353, 1952.

[31] D. Bohm and D. Pines, ”A Collective Description of Electron Interactions: III. Coulomb Interactions in a Degenerate Electron Gas”, Phys. Rev. 92, 609–625, 1953.

[32] S. L. Adler, ”Quantum theory of the dielectric constant in real solids”, Phys. Rev. 126, 413, 1962.

[33] N. Wiser, ”Dielectric constant with local field effects included”, Phys. Rev. 129, 62, 1963.

[34] H. Ehrenreich and M. H. Cohen, “Self-Consistent Field Approach to the Many-Electron Problem”, Phys. Rev. 115, 786, 1959.

[35] Bahn, S. R. & Jacobsen, K. W, “An object-oriented scripting interface to a legacy electronic structure code”, Computing in Science & Engineering 4, 56{66, 2002.

[36] Mortensen, J., Hansen, L. & Jacobsen, K, “Realspace grid implementation of the projector augmented wave method”, Physical review B 71, 035109, 2005.

[37] Ayse Berkdemir, Humberto R. Gutiérrez, Andrés R. Botello-Méndez, Néstor Perea-López, Ana Laura Elías, Chen-Ing Chia, Bei Wang, Vincent H. Crespi, Florentino López-Urías, Jean-Christophe Charlier, Humberto Terrones & Mauricio Terrones, “Identification of individual and few layers of WS_2 using Raman Spectroscopy”, Scientific Reports 3, Article number: 1755, 2013.

[38] Sanghyun Jo, Nicolas Ubrig, Helmuth Berger, Alexey B. Kuzmenko and Alberto F. Morpurgo, “Mono- and Bilayer WS_2 Light-Emitting Transistors”, Nano Lett, 14 (4), pp 2019–2025, 2014.

[39] Humberto R. Gutiérrez, Nestor Perea-López, Ana Laura Elías, Ayse Berkdemir, Bei Wang, Ruitao Lv, Florentino López-Urías, Vincent H. Crespi, Humberto Terrones and Mauricio Terrones, "Extraordinary room-temperature photoluminescence in WS_2 triangular monolayers", Nano Lett, 13 (8), pp 3447–3454, 2013.

[40] Beal, A. R. & Liang, W. Y. "Excitons in 2H-WSe_2 and 3R-WS_2", Journal of Physics C Solid State Physics 9, 2459–2466, 1976.

[41] Andrea Splendiani, Liang Sun, Yuanbo Zhang, Tianshu Li, Jonghwan Kim, Chi-Yung Chim, Giulia Galli and Feng Wang, "Emerging Photoluminescence in Monolayer MoS_2", Nano Lett, 10 (4), 1271−1275, 2010.

[42] Weijie Zhao, Zohreh Ghorannevis, Leiqiang Chua, Minglin Toh, Christian Kloc, Ping-Heng Tan, Goki Eda, "Evolution of Electronic Structure in Atomically Thin Sheets of WS_2 and WSe_2", ACS Nano, 7 (1), 791−797, 2013.

[43] Sefaattin Tongay, Jian Zhou, Can Ataca, Kelvin Lo, Tyler S. Matthews, Jingbo Li, Jeffrey C. Grossman and Junqiao Wu, "Thermally Driven Crossover from Indirect toward Direct Bandgap in 2D Semiconductors: $MoSe_2$ versus MoS_2", Nano Lett, 12 (11), pp 5576–5580, 2012.

[44] Won Seok Yun, S. W. Han, Soon Cheol Hong, In Gee Kim and J. D. Lee, "Thickness and strain effects on electronic structures of transition metal dichalcogenides: 2H-MX_2 semiconductors (M = Mo, W; X = S, Se, Te)", Phys. Rev. B 2012, 85 (3), 033305, 2012.

[45] A. Kuc, N. Zibouche and T. Heine "Influence of quantum confinement on the electronic structure of the transition metal sulfide TS_2", Phys. Rev. B 83, 245213, 2011.

[46] Hongliang Shi, Hui Pan, Yong-Wei Zhang and Boris I. Yakobson, "Quasiparticle band structures and optical properties of strained monolayer MoS2 and WS2", Phys. Rev. B, 87 (15), 155304, 2013.

[47] S. Horzum, H. Sahin, S. Cahangirov, P. Cudazzo, A. Rubio, T. Serin and F. M. Peeters, "Phonon softening and direct to indirect band gap crossover in strained single-layer $MoSe_2$", Phys. Rev. B, 87 (12), 125415, 2013.

[48] A. Klein, S. Tiefenbacher, V. Eyert, C. Pettenkofer and W. Jaegermann, "Electronic band structure of single-crystal and single-layer WS_2: Influence of interlayer van der Waals interactions", Phys. Rev. B, 64 (20), 205416, 2001.

[49] Allen MJ, Tung VC, Kaner RB, "Honeycomb Carbon : A Review of Graphene", Chem Rev, 110(1):132-45, 2010.

[50] A. H. Castro Neto, N. M. R. Peres, K. S. Novoselov, and A. K. Geim, "The electronic properties of graphene," Rev. Mod. Phys., vol. 81, no. 1, pp. 109–162, Jan. 2009.

[51] L. Hu & G. Gruner, ”Touch screen devices employing nanostructure networks”, US Pat. App. 11/552,834, 2013.

[52] V. M. Karpan, G. Giovannetti, P. A. Khomyakov, M. Talanana, A. A. Starikov, M. Zwierzycki, J. van den Brink, G. Brocks, and P. J. Kelly, ”Graphite and Graphene as Perfect Spin Filters”, Phys. Rev. Lett. 99, 2007.

[53] Ohta T, Bostwick A, Seyller T, Horn K, Rotenberg E, ”Controlling the Electronic Structure of Bilayer Graphene”, Science 313, 951, 2006.

[54] C. Lee, X. Wei, J. W. Kysar, and J. Hone, “Measurement of the Elastic Properties and Intrinsic Strength of Monolayer Graphene”, Science, vol. 321, no. 5887, pp. 385 –388, Jul. 2008.

[55] A. R. Ranjbartoreh, B. Wang, X. Shen, and G. Wang, “Advanced mechanical properties of graphene paper”, Journal of Applied Physics, vol. 109, no. 1, pp. 014306–014306–6, Jan. 2011.

[56] T. Ando, ”Exotic electronic and transport properties of graphene”, Phys. E 40, 213, 2007.

[57] K.I. Bolotin, K. Sikes, Z. Jiang, M. Klima, G. Fudenberg, J. Hone, P. Kim, and H. Stormer, “Ultrahigh electron mobility in suspended graphene”, Solid State Communications 146, 351, 2008.

[58] Thomas Mueller, Fengnian Xia & Phaedon Avouris, “Graphene photodetectors for high-speed optical communications”, Nature Photonics 4, 297, 2010.

[59] Wencan Jin, Po-Chun Yeh, Nader Zaki, Datong Zhang, Jerzy T. Sadowski, Abdullah Al-Mahboob, Arend M. van der Zande, Daniel A. Chenet, Jerry I. Dadap, Irving P. Herman, Peter Sutter, James Hone, and Richard M. Osgood, Jr, “Direct Measurement of the Thickness-Dependent Electronic Band Structure of MoS_2 Using Angle-Resolved Photoemission Spectroscopy”, Physical Review Letters 111, 106801, 2013.

[60] Aristea E. Maniadaki and Georgios Kopidakis, “Hydrogen on hybrid MoS_2/graphene nanostructures”, Phys. Status Solidi RRL 10, No. 6, 453–457, 2016.

[61] Wencan Jin, Po-Chun Yeh, Nader Zaki, Datong Zhang, Jonathan T. Liou, Jerzy T. Sadowski, Alexey Barinov, Mikhail Yablonskikh, Jerry I. Dadap, Peter Sutter, Irving P. Herman, and Richard M. Osgood, Jr, ”Substrate interactions with suspended and supported monolayer MoS_2: Angle-resolved photoemission spectroscopy”, Physical Review B 91, 121409, 2015.

[62] Oriol Lopez-Sanchez, Dominik Lembke, Metin Kayci, Aleksandra Radenovic, Andras Kis, “Ultrasensitive photodetectors based on monolayer MoS_2”, Nature nanotechnology 8, 497, 2013.

[63] Cristina E. Giusca, Ivan Rungger, Vishal Panchal, Christos Melios, Zhong Lin, Yu-Chuan Lin, Ethan Kahn, Ana Laura Elías, Joshua A. Robinson, Mauricio

Terrones, and Olga Kazakova, ”Excitonic Effects in Tungsten Disulfide Monolayers on Two-Layer Graphene” ACS Nano, 10 (8), pp 7840–7846, 2016.

[64] T. P. Kaloni, L. Kou, T. Frauenheim, and U. Schwingenschlögl, “Quantum spin Hall states in graphene interacting with WS_2 or WSe_2”, Appl. Phys. Lett. 105, 233112, 2014.

[65] Zheng Xin, Lang Zeng, Yijiao Wang, Kangliang Wei, Gang Du, Jinfeng Kang, and Xiaoyan Liu, ”Strain affected electronic properties of bilayer tungsten disulfide”, Japanese Journal of Applied Physics 53, 04EN06, 2014.

[66] Aristea E. Maniadaki, Georgios Kopidakis, Ioannis N. Remediakis, ”Strain engineering of electronic properties of transition metal dichalcogenide monolayers”, Solid State Communications, Volume 227, Pages 33-39, 2016.

[67] Debora Pierucci, Hugo Henck, Jose Avila, Adrian Balan, Carl H. Naylor, Gilles Patriarche, Yannick J. Dappe, Mathieu G. Silly, Fausto Sirotti, A. T. Charlie Johnson, Maria C.Asensio, and Abdelkarim Ouerghi, ”Band Alignment and Minigaps in Monolayer MoS_2-Graphene van der Waals Heterostructures”, Nano Lett, 16, 4054−4061, 2016.

[68] K. Ellmer, “Preparation routes based on magnetron sputtering for tungsten disulfide (WS_2) films for thin-film solar cells”, Physica Status Solidi (B) Basic Research, 245(9):1745-1760, 2008.

[69] Thanasis Georgiou, Rashid Jalil, Branson D Belle, Liam Britnell, Roman V Gorbachev, Sergey V Morozov, Yong-Jin Kim, Ali Gholinia, Sarah J Haigh, Oleg Makarovsky, Laurence Eaves, Leonid a Ponomarenko, Andre K Geim, Kostya S Novoselov, and Artem Mishchenko, ”Vertical field-effect transistor based on graphene-WS_2 heterostructures for flexible and transparent electronics”, Nature nanotechnology, 8(2):100-3, 2013.

[70] G. Onida, L. Reining and A. Rubio, “Electronic excitations: density-functional versus many-body Green’s-function approaches”, Rev. Mod. Phys. 74, 601, 2002.

[71] F. Huser, T. Olsen and K. S. Thygesen, ” How dielectric screening in two-dimensional crystals affects the convergence of excited-state calculations: Monolayer MoS_2”, Phys. Rev. B 88, 245309, 2013.

[72] Bairen Zhu, Xi Chen & Xiaodong Cui, “Exciton Binding Energy of Monolayer WS_2”, Scientific Reports 5, Article number: 9218, 2015.

[73] Toshihide Takagahara and Kyozaburo Takeda, “Theory of the quantum confinement effect on excitons in quantum dots of indirect-gap materials”, Physical Review B (Condensed Matter), Volume 46, Issue 23, pp.15578-15581, 1992.